NTIS # PB2015-

# SSC-469

# STRENGTH AND FATIGUE TESTING OF COMPOSITE PATCHES FOR SHIP PLATING FRACTURE REPAIR

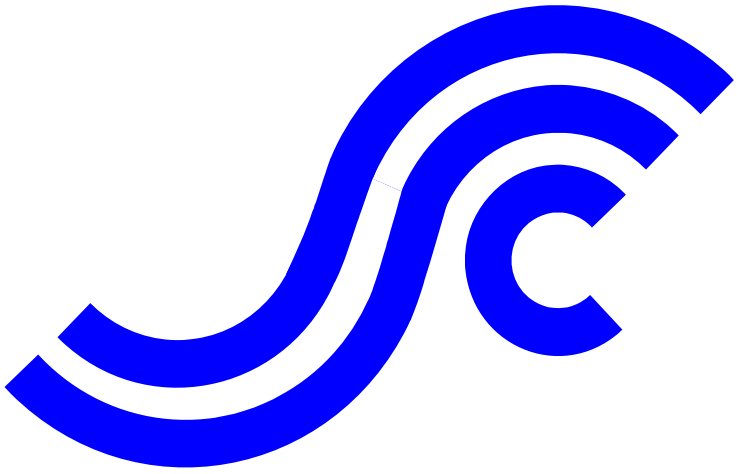



SHIP STRUCTURE COMMITTEE

2015

# Ship Structure Committee

RDML Joseph A. Servidio
U. S. Coast Guard Assistant Commandant,
for Prevention Policy
Co-Chair, Ship Structure Committee

RDML Bryant Fuller
Chief Engineer and Deputy Commander
For Naval Systems Engineering (SEA05)
Co-Chair, Ship Structure Committee

Mr. H. Paul Cojeen
Society of Naval Architects and Marine Engineers

Mr. Todd Grove
Senior Vice President
American Bureau of Shipping

Mr. John P. Quinn
Director, Office of Ship Construction
Maritime Administration

Ms. Julie Gascon
Executive Director, Domestic Vessel Regulatory Oversight and Boating Safety, Transport Canada

Mr. Kevin Baetsen
Director of Engineering
Military Sealift Command

Dr. Neil Pegg
Group Leader - Structural Mechanics
Defence Research & Development Canada - Atlantic

Mr. Jeffrey Lantz,
Director, Commercial Regulations and Standards
U.S. Coast Guard

Mr. Matthew Garner
Director, Structural Integrity and Performance Division
Naval Sea Systems Command

Mr. Albert Curry
Deputy Assistant Commandant for Engineering and Logistics – U.S. Coast Guard

Dr. John Pazik
Director, Ship Systems and Engineering Research Division
Office of Naval Research

## SHIP STRUCTURE SUB-COMMITTEE

**AMERICAN BUREAU OF SHIPPING (ABS)**

Mr. Craig Bone
Mr. Daniel LaMere
Mr. Richard Delpizzo

**DEFENCE RESEARCH & DEVELOPMENT CANADA ATLANTIC (DRDC)**
Mr. Malcolm Smith
Mr. Cameron Munro
Dr. Layton Gilroy

**MARITIME ADMINISTRATION (MARAD)**
Mr. Chao Lin
Mr. Richard Sonnenschein
Mr. Todd Ripley
Mr. Todd Hiller

**MILITARY SEALIFT COMMAND (MSC)**
Michael Touma

**NAVSEA/ NSWCCD**
Mr. David Qualley
Mr. Gerard Mercier
Mr. Dean Schleicher

**TRANSPORT CANADA**
Mr. Ian Campbell
Mr. Bashir Ahmed Golam

**UNITED STATES COAST GUARD (CVE)**

CAPT John Mauger
Mr. Jaideep Sirkar
Mr. Charles Rawson

**SOCIETY OF NAVAL ARCHITECTS AND MARINE ENGINEERS (SNAME)**
Mr. Rick Ashcroft
Mr. Alex Landsburg
Mr. Dave Helgerson
Mr. Paul H. Miller

**UNITED STATES COAST GUARD (ELC)**
CAPT NATE MOORE
MR. FRANK DEBORD

**OFFICE OF NAVAL RESEARCH (ONR)**
Dr. Paul Hess

Member Agencies:

*American Bureau of Shipping*
*Defence Research and Development Canada*
*Maritime Administration*
*Military Sealift Command*
*Naval Sea Systems Command*
*Office of Naval Research*
*Society of Naval Architects & Marine Engineers*
*Transport Canada*
*United States Coast Guard*

Ship
Structure
Committee

Address Correspondence to:

COMMANDANT (CG-ENG-2/SSC)
ATTN (EXECUTIVE DIRECTOR/SHIP
STRUCTURE COMMITTEE)
US COAST GUARD
2703 MARTIN LUTHER KING JR. AVE SE
WASHINGTON DC 20593-7509
Website: http://www.shipstructure.org

**SSC – 469**
**SR – 1461**

**March 03, 2015**

**STRENGTH AND FATIGUE TESTING OF COMPOSITE PATCHES FOR SHIP PLATING FRACTURE REPAIR**

The objective of this research project is to examine, through physical testing and numerical simulations, the use of composite patches for preventing crack growth and extending the service life of ship plating. This study examines the repair of cracked ship plating using composite patches, particularly when subjected to cycling loads.

Fatigue growth of fractures is a common problem for structures operating in the marine environment. A flaw or fracture may grow due to repetitive, cyclic loadings caused by the sea state, weather, and payload distribution, etc.

Analytical capabilities exist for predicting the effectiveness of the composite patch configuration, but such analyses demand specific idealizations and assumptions that must be validated experimentally in order for this technology to be used in practice.

Specimens were tested with and without the use of composite reinforcements in order to corroborate finite element analyses. The results of our numerical analysis studies concludes that the finite element method can be used very effectively with accurate predictions of crack growth, particularly for the unpatched plates.

We thank the authors and Project Technical Committee for their dedication and research toward completing the objectives and tasks detailed throughout this paper and continuing the Ship Structure Committee's mission to enhance the safety of life at sea.

PAUL F. THOMAS
Rear Admiral, U.S. Coast Guard
Co-Chairman, Ship Structure Committee

L. BRYANT FULLER
Rear Admiral, U.S. Navy
Co-Chairman, Ship Structure Committee

**Technical Report Documentation Page**

| | | |
|---|---|---|
| 1. Report No. SSC - 469 | 2. Government Accession No. | 3. Recipient's Catalog No. |
| 4. Title and Subtitle<br>STRENGTH AND FATIGUE TESTING OF COMPOSITE PATCHES FOR SHIP PLATING FRACTURE REPAIR | | 5. Report Date<br>03/03/2015<br>6. Performing Organization Code |
| 7. Author(s)<br>Karr, D.G.; Baloglu, C.; Cao, T.J.; Douglas, A.; Nielsen, K.; Ong, K.T.; Rohrback, B.; and Si, N. | | 8. Performing Organization Report No.<br>SR - 1461 |
| 9. Performing Organization Name and Address<br>Department of Naval Architecture and Marine Engineering<br>University of Michigan<br>Ann Arbor Michigan 48109-2145 | | 10. Work Unit No. (TRAIS)<br>11. Contract or Grant No.<br>N00178-04-D-4023 FD01 |
| 12. Sponsoring Agency Name and Address<br>Ship Structure Committee<br>U.S. Coast Guard (G-ENG-2/SSC)<br>2703 Martin Luther King Jr. Ave SE<br>Washington, DC 20593-7509 | | 13. Type of Report and Period Covered<br>Final Report<br>4/2011- 9/2014<br>14. Sponsoring Agency Code<br>CG-5P |
| 15. Supplementary Notes<br>Sponsored by the Ship Structure Committee and its member agencies. Reviewed by designated Project Technical Committee | | |


**16. Abstract**

The objective of this research project is to examine, through physical testing and numerical simulations, the use of composite patches for preventing crack growth and extending the service life of ship plating. Fatigue tests were conducted on the steel plates to experimentally validate the effectiveness of using composite patches as a means to prevent crack growth and extend the fatigue life of structural components. Specimens were tested with and without the use of composite reinforcements in order to corroborate finite element analyses. The results of our numerical analysis studies concludes that the finite element method can be used very effectively with accurate predictions of crack growth, particularly for the unpatched plates. Numerical simulations of the cracked plates with composite patches indicate roughly two orders of magnitude increase in service life for the conditions tested although test results show increases closer to a single order of magnitude increase. This difference is attributed to two factors: failure mechanisms associated with the debonding of the patch and the actual cracking of the patch itself. Of critical importance therefore are the implementation of a quality-controlled bonding procedure and optimization of the geometry and properties of the patch systems dependent upon the parent plate's properties and fracture conditions.


| | | | |
|---|---|---|---|
| 17. Key Words<br>Finite Element Analysis, Fatigue, Crack, Composite, Fracture, Arrestor, Stress Concentration FRP, Ship Structure, Service Life | 18. Distribution Statement<br>Distribution unlimited, available from:<br>National Technical Information Service<br>Springfield, VA 22161<br>703 487 4650 | | |
| 19. Security Classif. (of this report)<br>Unclassified | 20. Security Classif. (of this page)<br>Unclassified | 21. No. of Pages<br>74 | 22. Price |

**CONVERSION FACTORS**
**(Approximate conversions to metric measures)**

| To convert from | to | Function | Value |
|---|---|---|---|
| **LENGTH** | | | |
| inches | meters | divide | 39.3701 |
| inches | millimeters | multiply by | 25.4000 |
| feet | meters | divide by | 3.2808 |
| **VOLUME** | | | |
| cubic feet | cubic meters | divide by | 35.3149 |
| cubic inches | cubic meters | divide by | 61,024 |
| **SECTION MODULUS** | | | |
| $inches^2$ $feet^2$ | $centimeters^2$ $meters^2$ | multiply by | 1.9665 |
| $inches^2$ $feet^2$ | $centimeters^3$ | multiply by | 196.6448 |
| $inches^4$ | $centimeters^3$ | multiply by | 16.3871 |
| **MOMENT OF INERTIA** | | | |
| $inches^2$ $feet^2$ | $centimeters^2$ $meters^2$ | divide by | 1.6684 |
| $inches^2$ $feet^2$ | $centimeters^4$ | multiply by | 5993.73 |
| $inches^4$ | $centimeters^4$ | multiply by | 41.623 |
| **FORCE OR MASS** | | | |
| long tons | tonne | multiply by | 1.0160 |
| long tons | kilograms | multiply by | 1016.047 |
| pounds | tonnes | divide by | 2204.62 |
| pounds | kilograms | divide by | 2.2046 |
| pounds | Newtons | multiply by | 4.4482 |
| **PRESSURE OR STRESS** | | | |
| pounds/inch2 | Newtons/$meter^2$ (Pascals) | multiply by | 6894.757 |
| kilo pounds/$inch^2$ | mega Newtons/$meter^2$ (mega Pascals) | multiply by | 6.8947 |
| **BENDING OR TORQUE** | | | |
| foot tons | meter tons | divide by | 3.2291 |
| foot pounds | kilogram meters | divide by | 7.23285 |
| foot pounds | Newton meters | multiply by | 1.35582 |
| **ENERGY** | | | |
| foot pounds | Joules | multiply by | 1.355826 |
| **STRESS INTENSITY** | | | |
| kilo pound/$inch_2$ $inch^{1/2}$ ($ksi\sqrt{in}$) | mega Newton $MNm_{3/2}$ | multiply by | 1.0998 |
| **J-INTEGRAL** | | | |
| kilo pound/inch | Joules/$mm_2$ | multiply by | 0.1753 |
| kilo pound/inch | Kilo Joules/$m_2$ | multiply by | 175.3 |

# Table of Contents

# 1. Introduction

The aims of this research are to explore and experimentally validate the use of composite patches for preventing crack growth and extending the lifetime of aluminum and steel ship structures. A composite patch works as a crack arrestor by decreasing the stress in the area of the crack tip. Analytical capabilities exist for predicting the effectiveness of the composite patch configuration, but such analyses demand specific idealizations and assumptions that must be validated experimentally in order for this technology to be used in practice. This project thus contributes to the development of this technology as a useful and reliable tool for ship plating fracture repair and seeks to foster its industrial acceptance and implementation.

Funding for this Project was awarded from the Ship Structure Committee through the Naval Surface Warfare Center, Carderock Division and subsequently through BMT Designers and Planners to the University of Michigan.

Two configurations were investigated. Steel plates having a length of 18.0 in, a width of 12.0 in, and a thickness of 0.25 in, with a 3.0 inches initial crack at mid span were first studied without the use of reinforcements. Other plates of similar geometry were then examined using double-sided reinforcements. A cyclic load oscillating between 2.0 and 50.0 kips was applied at one end of the plates. Prior to these tests, simple tensile strength tests were conducted to establish the material properties of the composite patches and the steel panels.

Tests were conducted on the steel plates to experimentally validate the effectiveness of using composite patches as a means to prevent crack growth and extend the fatigue life of structural components. Specimens were tested with and without the use of reinforcements in order to corroborate finite element analyses. It is concluded that the finite element method can be used very effectively with accurate predictions of crack growth particularly for the unpatched plates. Finite element analyses, test results and analytical formulations ( e.g. using the correction factors of Boresi et al.) agree remarkably well.

Numerical simulations of the cracked plates indicate roughly two orders of magnitude increase in service life for the conditions tested although test results show increases closer to a single order of magnitude increase. This difference is attributed to two factors: debonding of the patch and actual cracking of the patch. Neither of these failure modes was taken into account in the finite element analyses. The debonding of the patch can also be improved by careful attention to the quality of the bonding process. The effectiveness composite patching of steel plates has been demonstrated in this project. For improvements in results however are believed to be achievable; of critical importance are two factors: implementation of a quality-controlled bonding procedure and optimization of the geometry and properties of the patch systems dependent upon the parent plate's properties and fracture conditions.

# 2. Objective and Scope

Fatigue growth of fractures is an all-too-common problem for structures operating in the marine environment. A flaw or fracture may grow due to repetitive, cyclic loadings caused by the sea state, weather, and payload distribution, etc.

Cracks are often repaired by welding. More permanent repairs frequently require the ship's plate to cropped and renewed. However, welding will change the property of the material and could create additional stress concentrations and may also have poorer fatigue performance than the original material. More importantly, not all locations can be welded easily, such as locations behind pipes, inside or near fuel tanks, etc.

This study examines the repair of cracked ship plating using composite patches particularly when subjected to cycling loads. The use of adhesively bonded composite patches for repairing cracked or corroded structural components has experienced a significant increase in both aircraft and ship structures. Earlier studies in this area were conducted by Allan, Bird and Clarke [1988]. A more recent review of strengthening of steel components was provided by Zhao and Zhang [2007]. Although this method may still be in early stages, particularly in terms of applications, it has been recognized to be an efficient and economical approach to enhance the service life of various structural members. A more general review of the use of composites in the marine environment can be found in Shenoi et al. [2011]. As mentioned, the purpose of this research is to explore and experimentally validate the use of composite patches for preventing crack growth and extending the lifetime of aluminum and steel ship structures. Its objective is to predict and validate the effectiveness of composite patch configurations as a useful and reliable tool for fracture repair. The project involved undertaking the following tasks.

**Task 1** ***Develop Finite Element Analyses***

A finite element analysis shall examine steel plate systems to supplement the data for existing analysis of aluminum plate systems.

**Task 2** ***Conduct Analyses***

A finite element analysis shall predict strength, crack growth and patch failure on steel and aluminum plate repair systems for both single sided and two sided repair options for a variety of composite patches that are compatible for use in the marine environment. The assumed plate thicknesses and associated loads should include a range that would be consistent with those found on large commercial vessels. Additionally, for a patch/plate system to be viable alternative in the marine industry a relatively short cure time is needed. When selecting the composite patch material and epoxy, due regard shall be given to the patch cure time and potential corrosion effects on the base plate.

**Task 3** ***Perform Strength and Fatigue Tests***

Plate/patch/crack systems shall be created and tested. Video and/or photographic documentation shall be used to supplement empirical data to demonstrate the plate/patch performance. Any substantial deviations between the test results and the prediction from the finite element analysis shall be addressed before additional tests are completed.

**Task 4** ***Develop and Document Final Results***

The final results shall thoroughly address the findings and document the process used during the project.

# 3. Background

As part of this SSC project, a preliminary study was undertaken to establish the typical grades of steel and aluminum and associated plate thickness being used in ship construction. Personnel at the U.S. Coast Guard, the U.S. Navy and the American Bureau of Shipping (ABS) were contacted for information and recommendation. In total, 11 engineers and technical representatives at these agencies were contacted and their willingness to share their expertise in this area is greatly appreciated.

Both the U.S. Coast Guard and U.S. Navy provided the grades of aluminum and steel commonly used in their fleet with the respective thicknesses. The ABS recommended using ASTM 36 steel as it is most commonly used in shipbuilding. The ABS also recommended conducting the experiments with fracture sizes in the range of 30mm to 50mm.

Some photographs of fracture on shipboard plating are shown in Appendix A. While some of these fractures occur on flat plates, many other fractures started at welded regions and propagated to the adjacent areas.

# 4. Literature Review

Adhesively bonded patch repairs are increasingly being used for cracked or corroded structural components in ship repairs and aircraft structures to enhance the service life. There are some advantages that make composite patches ideal reinforcement for structural repairs, which are high specific strength and stiffness, reduced repair time and lower cost, lightweight, anti-corrosion and anti-fretting properties. Also the patches can be fabricated in different sizes and shapes to conform the complicated shapes of the structures.

Lam et al. [2010] found from their experimental and numerical studies that the stress intensity factors for cracked steel plates were substantially reduced by the application of composite patching. They used carbon reinforced plastic patches and found a strong dependence on the number of layers and less effect from changes in patch widths and length. This further implies that fatigue life would be enhanced due to the reduction of stress intensity. The works of Colombi et al. [2002] also find sensitivity to adhesive layer thickness and prestress in the composite patches regarding the reduction is stress intensity factors for composite reinforced steel. It should be noted that efforts are also undertaken for the use of composite patches to strengthen steel components without pre-cracks. Bocciarelli et al. [2009] used double sided composite patches to study the fatigue performance of steel members in tension.

The fatigue life of notched steel girders reinforced with composite patches was studied by Tavakkolizadeh and Sasadatmanesh [2003]. They found a three-fold increase in fatigue life over the non-reinforced steel. These tests were performed at moderate stress levels and up to several hundred thousand cycles to failure. Similarly, Huawen et al. [2010] found a four-fold increase in fatigue life of strengthened steel plating with failure in the several hundred thousand cycle range.

Carbon/epoxy patches we used by Tsouvalis, Mirisiotis and Dimou on cracked steel plating, also tested in fatigue. They found a two-fold increase in specimen life lower-cycle fatigue in the range of several tens of thousands of cycles. Debonding was the initiating failure mode in their experimental study. Their analytical study indicated the importance of adhesive strength and relative stiffness of the patches. Liu and colleagues [2009a, b] conducted fatigue tests and reported their analytical studies for steel plates reinforced with carbon fiber composite patches subject to higher cycle fatigue in the range of a million cycles. Fatigue life was again increased several fold.

Khalili et al. [2009, 2010] studied edge-cracked aluminum plates repaired with one-sided composite patches experimentally for their response to Charpy impact test. The specimens were made of AA 1050 aluminum alloy sheets with a 2 mm thickness. For composite patches two different materials were used, in one the reinforcement was woven glass-fibers while the other

had woven carbon fibers as the reinforcement. 3-ply and 5-ply composite patches were used in each case. As adhesive for bonding Araldite 2015 was used. Before bonding the patch to the cracked specimens the surfaces were prepared according to the procedure recommended by American Society for Testing and Materials (ASTM) standards. Finally it was concluded that carbon patches are more effective in reinforcing the cracked plates than glass patches, the carbon fiber patches show better characteristics than glass-fiber patches when the ratio of crack length to specimen width is constant, and increasing the number of layers from three to five has only a small effect on energy absorption.

Grabovac and Whittaker [2009] examined the carbon fiber composite overlays (patches) installed on a Royal Australian Navy frigate to inhibit the recurrence of superstructure fatigue cracking. The composite patches installed on HMS Sydney frigate in 1993, and after that time the ship has successfully served for more than 15 years and has gone through several complete maintenance cycles. This paper addresses service history of the ship and a total of four repairs that were made to the composite overlays. The background, the materials used to prepare the composite patches, and adhesives are discussed in another paper by the same author, which will be explained later in this report. The authors concluded that the patches are durable enough even for a service life of more than 15 years on a weather deck in a very harsh ocean environment, easily repairable, effortlessly removable by using an abrasive blasting equipment and easily accessible to survey the structure behind the patches.

Xiong and Shenoi [2008] outlined an experimental screening procedure for bonded composite patch repair scheme for cracked aluminum alloy panels based on static and fatigue strength concepts. They investigated static and fatigue behavior of different patch materials thicknesses. The materials used in this investigation included LY12 aluminum alloy as the substrate, SY-24C as the adhesive system and T300/3234, G803/3242 and SW220/2322 fiber/epoxy prepregs as the patch materials. The substrates were machined into the panels with the dimensions of 350 mm length, 60 mm width and 2.4 mm thickness. Surface preparation of the substrates was done prior to the adhesive bonding of the patches. All patches were formed with tapers on the longitudinal ends by using plies of decreasing lengths from the bonded surface to the top with a cover ply, as is usually done in actual applications. The authors confirmed that the thickness of the patch has a significant influence on static and fatigue strengths of the repaired specimen. An appropriate thickness of bonding patch can significantly enhance static and fatigue properties of repaired specimen. Three different kinds of fiber reinforced patches with the same thickness lead to the close static strengths but different fatigue properties. The fiber reinforced composite material of patch has a slight influence on static strength but a significant effect on fatigue property.

Hosseini-Toudeshky et al. [2007] investigated the numerical and experimental fatigue crack growth behavior of centrally cracked aluminum panels in mode-I condition repaired with single-side composite patches. The center cracked panels were made of 2024-T3 aluminum alloy. The patches were made of glass/epoxy (by Hexcel Composites) composite with a perpendicular lay-up configuration to the crack length. Two different groups of specimen with thickness of 2.24

mm and 6.35 mm were tested with 4, 8, 16 layers of patch. It was shown that the crack growth life of the panel with the thickness of 2.29 mm increases as the number of plies increases. However for the panel with the thickness of 6.35 mm increasing number of patch layers has not a significant effect on the life extension. Therefore, single-sided repair of thin panels using composite patch is more efficient than the thick panels.

In their study, Harris and Olshenske [2010] evaluated the benefits of utilizing a new aligned, discontinuous formable textile called DiscoTex® (in development by Pepin Associates) for producing laminate patches for bonded repairs on selected double curvature composite shapes typical of those geometries found on fixed wing fighter aircraft. DiscoTex® minimizes labor costs by eliminating cutting and darting associated with traditional continuous fiber/tow textile lay-up methods, because it can stretch over complex shapes and intricate geometries from simple starting shapes such as flat plates or tubes. In the first part of the experiments, the processing behavior and final material quality (mechanical, porosity, and resin content) of flat laminate patches fabricated from standard continuous carbon fiber based fabric and DiscoTex® fabric using typical wet lay-up repair procedures were compared. The second part was related to the formability behavior DiscoTex® over complex curved composite surfaces. The patches were fabricated from EA9390/aS4 and EA9390/AS4 DiscoTex® materials using 9-plies. Conclusively, the basic material properties and characteristics of DiscoTex® fabric are in the same spectra as current repair materials.

Wang et al. [2006] evaluated the fatigue crack behavior of notched 7075 and 6061 aluminum alloy substrates in the gigacycle regime. The composite patch was comprised of Textron's 5521 boron/epoxy prepreg tape. A 3M manufactured AF-163-2K adhesive film was used to bond the patches to the substrate. Three composite patches with 1-ply, 2-ply, and 4-ply were studied. It was noticed that composite patch repair improves the fatigue life of the substrates considerably. The crack growth was generally retarded with plying. Conclusively, the effectiveness of the composite repair in significantly increasing the fatigue life of the notched substrates has been experimentally verified.

Okafor et al. [2005] investigated the design, analysis, and durability of adhesively bonded composite patch repairs of cracked aluminum panels. Both experimental results and FEM analyses were compared. Centrally pre-cracked 2024-T3 clad aluminum panels with dimensions of 381 x 89 x 1.6 mm were used as substrates. For FEM the composite patch was designed using the CRAS v0.3 developed by United States Air Force. For experiments the patches were fabricated from boron/epoxy 5521 prepreg (Textron Specialty Materials Inc.). The edges of the patches were tapered to reduce the peel stresses. Two different patch configurations with 5 and 6 plies were considered. The patches were applied to the aluminum panel using FM-73 (Cytec Fiberite) adhesive. Surface preparation consisted of degreasing the aluminum panels with acetone followed by grit blasting and application of primer. The patches were fabricated and applied to the aluminum panels by Integrated Technologies Inc. in Bothell Washington. From the results of the research it was concluded that maximum skin stress decreases after the application

of the patch, and the shear stresses in the adhesive are higher for the 5-ply patch as compared to the 6-ply patch, which indicated that 5-ply patch will fail earlier.

Turton et al. [2005] reported the case studies of QinetiQ's marine patch repair work. QinetiQ has patch repaired Type 21 frigates, Type 42 destroyers, offshore oil platforms as well as developing a number of other composite repair techniques to marine structures. Patch fabrication techniques of hand lay-up, resin infusion and prepreg were trialed and the advantages and disadvantages of the methods are discussed. The authors explained the composite patch application procedure, advantages of patch repair and three case studies. Finally they listed hand lay-up advantages and disadvantages, resin infusion advantages and disadvantages and prepreg advantages and disadvantages according to their experience throughout the patch repair work on frigates, destroyers and oil platforms.

Grabovac [2003 described a project carried out by the Defence Science and Technology Organization (DSTO) for the Royal Australian Navy (RAN) in which the principal objective was to investigate the sustainability of bonded composite technology to reinforce part of a ship superstructure prone to fatigue-induced cracking. Patch repair performed on the 02 deck of RAN frigate HMAS Sydney between frames of 188 and 212. The frigate has a steel hull with a continuously welded aluminum alloy (5456) superstructure extending over about 55% of the ship's length. The composite reinforcement was made using a modified epoxy vinyl ester and 25 plies of unidirectional carbon fiber. Because a resin system which is able to provide strong, durable adhesion and sustain oscillating service loads was not available during the time of the repair, a DSTO-developed resin system was used. Surface preparation of the 02 deck included removal of the surface coating and preparations for grit blasting. After the patches were applied, the surface finish comprised of a two-coat coverage of an epoxy-based primer, a standard navy paint scheme and the final non-skid layer. Conclusively, no requirement for metal repairs (re-welding, doublers) needed in the area, removal and reassembly of lagging, pipes, cables were not necessary for the repair and labor and material costs were reduced compared to metal repairs.

Seo and Lee [2002] investigated the fatigue crack growth behavior of cracked aluminum plate repaired with bonded composite patch especially in thick plate through experimental and numerical study. Two types of crack front modeling, i.e. uniform crack front model and skew crack front model, were used. Specimens were machined from aluminum sheet (Al 7075T6) in dimensions of 220 mm long x 70 mm wide x 10 mm thick. Before the composite patch repair, fatigue loading for precracking was applied. A graphite/epoxy composite patch was made using 8 layers of unidirectional prepreg. The patch was cured using an autoclave and bonded to the cracked specimen using epoxy film adhesive. Conclusively, the authors compared the stress intensity factor calculated using FEM with the experimentally determined results.

Wang and Pidaparti [2002] reported monotonic tensile and fatigue crack growth studies conducted on 7075-T6 Al substrates with and without bonded boron/epoxy patches. The dimensions of the substrates were 305 mm long x 51 mm wide x 1.6 mm thick. The composite

patch was Textron's 5521 boron-epoxy prepreg tape. The 3M manufactured AF-163-2K adhesive was used to bond the patches to the substrate. 1-, 2-, and 4-ply patches were compared. It was shown experimentally and analytically that the fatigue lifetime of the repaired substrates is increased as the number of plies increases.

Schubbe and Mall [1999] conducted an experimental investigation to characterize the post-repair fatigue crack growth behavior in 6.350 mm thick 2024-T3 aluminum panels repaired with the asymmetrically bonded full width boron/epoxy composite patch. The characteristics of the repaired thick panel (6.35 mm) were compared with the repaired thin panel (3.175 mm). The specimens were machined 508 mm long x 153 mm wide with a central crack. FM-73 sheet adhesive was used to bond the patches to the specimens. Steps in preparation of the surfaces included: Solvent degreasing, grit blasting (mechanical abrasion), silane agent preparation, wetstanding procedure (silane application), primer application and cure. Methyl ethyl ketone was used as a degreaser on the surfaces. Conclusively, asymmetric repair of the cracked panels with bonded composite patch extended their fatigue lives.

Denney and Mall [1997] investigated the effects of debonds on the fatigue response of cracked aluminum panels repaired with bonded composite patches. The specimens used in this study were designed and fabricated to simulate the repair of an aircraft fuselage. Aluminum panels of 2024-T3 Alclad in dimensions of 508 mm x 152 mm x 1 mm were fabricated with a nominal 25.4 mm fatigue crack perpendicular to their longest dimension (load direction). The bonded reinforcement was a 3-ply unidirectional boron/epoxy reinforcement with fibers in the loading direction by Textron Speciality Materials Incorporated. The matrix was 5521 resin. The adhesive was AF-163-2M film adhesive manufactured by 3M Incorporated. The patches were applied only one side of the panels over the fatigue crack. The authors examined the effects of debond location and the effects of disbond size on patching efficiency. The conclusions of this study are: Debonding over the crack result in greater crack growth rates and shorter fatigue lives as compared to debonds away from the crack and the disbonds away from the crack do not reduce patch efficiency.

Grabovac, Bartholomeusz, and Baker [1993] described the efforts to develop a carbon fiber composite doubler to reinforce the aluminum alloy deck superstructure of a Royal Australian Navy FFG-7 frigate. The paper gives an overall description of the project to date, dealing with the design of the reinforcement; the materials selection; development and characterization of the matrix, composite and adhesive bond. 25 mm thick aluminum alloy 5083 was used for the experiments although 5456 was used to construct the ship; however both alloys have similar mechanical properties. The liquid-resin application process had the considerable advantage of avoiding storage problems as no reaction can occur until the resin components are mixed together. In contrast, the prepreg poses severe storage problems because of low temperature cure characteristics. Based on these considerations it was decided to adopt the wet lay-up resin application process. According to the authors' experiences ambient or near-ambient temperature curing epoxies tend to be brittle, the peel strength which is indicative of resin toughness is

dependent on the rubber concentration of the resin, and the vinyl ester resin has longer pot life, higher resin flow, better fiber wet-out, and ambient cure temperature properties that are valuable for open deck repairs on ships.

Allan, Bird, and Clarke [1988] suggested the use of adhesives in repair of cracks in ship structures and listed the design considerations of the patches for ships. Boron fibers were suggested since this material could be bonded to the aluminum plate in sufficient thickness to achieve the required reduction in stress level, the patch could be tapered to avoid imposing a local stress concentration at the patch boundary. Patch materials and adhesives were listed as Permabond E04 and E32 patches, Ciba-Geigy 1927 epoxy resin and Permabond F241 acrylic adhesive. Because the preparation of adherend surfaces onboard ship is limited, using a commercial low toxicity solvent such as Genklene (1:1:1 trichloroethane) applied by wiping with lint free clothes, followed by grit blasting with 60/80 size alumina grit to produce a clean, bare metal surface was recommended.

Bone in his Master's Thesis [2002] tested pre-impregnated and wet lay-up processes and single and double- sided patches. For the experiments 7075-T6 aluminum alloy plates in dimensions of 12 in. x 12 in. x 1/8 in. and 12 in. x 12 in. x 1/16 in. with edge cracks were chosen. The graphite fiber used in the experiments was unidirectional GA060 donated by Wahoo Composites and the resin and hardener system was Pro-set 125 Resin/226 Hardener donated by Gougen Brothers. As adhesive layer FM73 donated by Cytec Industries was employed. For wet lay-up process an aluminum etching system donated by Gougen Brothers was utilized. The surfaces were cleaned using acetone alone. Two different epoxies were used, one of them was a product JB Weld, and the other was Epoxy-Patch 1105 High Peel by Dexter Corporation's Adhesive & Structural Materials Division.

Finally, the success of a bonding repair depends on the properties of the adhesive and the patch, and its affinity for the substrates. The quality of the bond also depends upon bonding procedure and surface preparation. As it can be concluded above discussions, for aluminum substrates boron-epoxy, carbon-epoxy, and graphite-epoxy have been mostly used to be repair patches. The performance of the adhesive plays a key role in the success of the bonded composite patch repairs (see also, for example, Buyykozturk et al., 2003). In our experiments we also found that debonding was a key failure mechanism which limited fatigue strength for the composite patching approach.

# 5. Preliminary Finite Element Modeling

The aim of Project 469: Composite Patches for Ship Repair is to explore and experimentally validate the use of composite patches in preventing crack growth, and extending the lifespan of aluminum and steel ship structures. The first step is performing finite element analysis (FEA) on composite patches on metal plates. The commercial software used is *ABAQUS*. The results from the finite element modeling were first validated with previous data Edwards [1999] and Edwards and Karr [1999], who used *ANSYS*. This section assesses the credibility of the *ABAQUS* model for subsequent modeling of test configurations.

## 5.1 Finite Element Analysis Model

The preliminary FEA model is a square plate 36in in length. The plate thicknesses are 0.5 in and 0.75 in. Note the eventual plate thickness for the tests were 0.25 in due to limitations of the test facilities. The modeled plate material is high carbon steel. The composite patches used are Boron/Epoxy and Carbon/Epoxy. The patch configuration is a double patch, i.e. one on each side of the plate. The thickness of the composite patch and adhesive are 0.04in and 0.0039in respectively. The load used is 30ksi as a far-field prescribed stress level. Refer to Table 5-1 for the material properties and Figure 5-1 for the FEA model geometry.

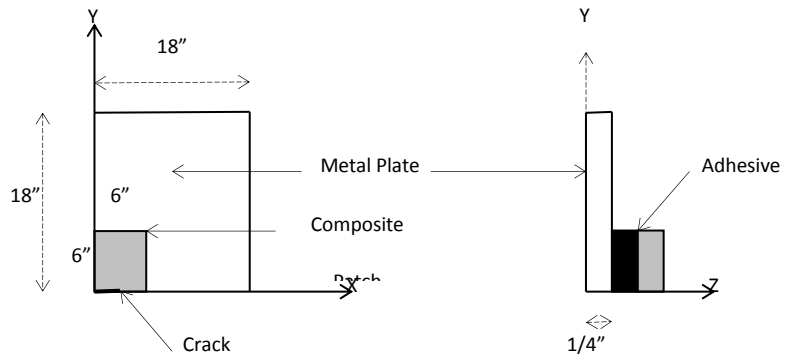


**Figure 5-1: Reduced FEA Model**

**Table 5-1: Finite Element Material Properties**

| Property | HTS Steel | Gr/Ep | Br/Ep | Adhesive |
|---|---|---|---|---|
| $E_x$, Msi | 30.0 | 1.41 | 3.68 | 0.28 |
| $E_y$, Msi | 30.0 | 20.0 | 30.2 | 0.28 |
| $E_z$, Msi | 30.0 | 1.41 | 3.68 | 0.28 |
| $G_{xy}$, Msi | 11.5 | 1.0 | 1.04 | 0.11 |
| $G_{xz}$, Msi | 11.5 | 0.46 | 0.71 | 0.11 |
| $G_{xy}$, Msi | 11.5 | 1.0 | 0.71 | 0.11 |
| $\nu_{xy}$ | 0.30 | 0.30 | 0.17 | 0.27 |
| $\nu_{xz}$ | 0.30 | 0.49 | 0.40 | 0.27 |
| $\nu_{yz}$ | 0.30 | 0.30 | 0.17 | 0.27 |

## 5.2 Theoretical Comparisons – Unpatched Plates

The main focus of the preliminary FEA modeling effort is to determine the stress intensity factor for Mode I fracture, $K_I$. The theoretical basis lies with the limit of an elliptical crack, Figure 5-2, as the aspect ratio reaches that of the idealized flat crack. Roy, Lang, and May [2009] and Righiniotis, et al. [2004] provide also the application of fracture mechanics concepts to the modeling analysis of patched steel plating. Our approach, described subsequently in section 5.3, is similar to their descriptions.

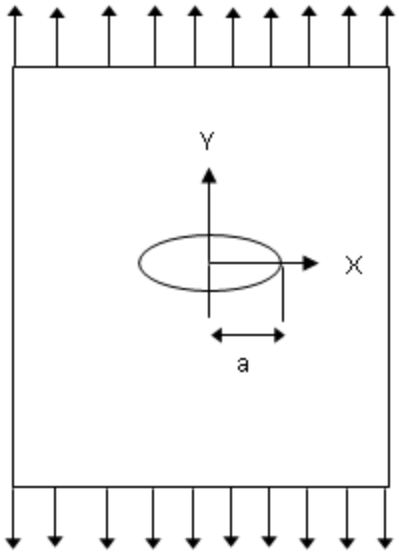


**Figure 5-2: Illustration of an Central Elliptical Crack with Far-Field Stress.**

In general, the stress intensity factor for a center crack in a finite plate (Figure 5-3) is expressed with a geometric correction factor (Y) as follows [see for example Wiernicki, 1995],

$$K_I = Y\sigma\sqrt{\pi a} \tag{5.1}$$

where σ is the far-field stress, a is the half crack length and $K_I$ has dimensions $\frac{force}{length^{1.5}}$.

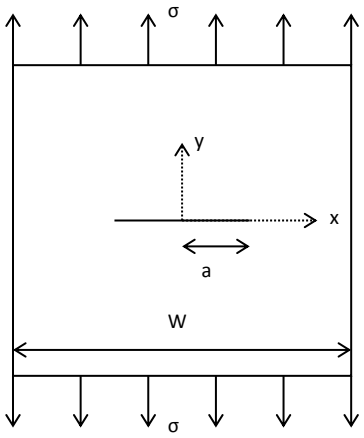


**Figure 5-3: Flat Central Crack in a Finite Plate**

Several forms have been proposed for the geometric correction factor Y:

$$\text{Brock: } Y = \sec\sqrt{\frac{\pi a}{W}}$$

$$\text{Wiernicki: } Y = \sqrt{\sec\frac{\pi a}{W}} \tag{5.2}$$

$$\text{Boresi: } Y = f(\lambda), \text{ where } \lambda = \frac{4a}{W} \text{ (see Table 5-)}$$

Results for the different forms of corrected stress intensity factors are plotted in Figure 5-4. The FEA results for 0.5in and 0.75in steel plate without patch are also included. Also the stress intensity factors plotted agree very well in both trend and range of values with the results from Edwards and Edwards and Karr [1999]. The Boresi correction factor is limited to small crack lengths ( $\frac{2a}{W} < 0.3$ ).

**Table 5-2: Stress Correction Factor – Central Crack**

| λ | f(λ) |
|---|---|
| 0.1 | 1.01 |
| 0.2 | 1.03 |
| 0.3 | 1.06 |
| 0.4 | 1.11 |
| 0.5 | 1.19 |
| 0.6 | 1.3 |

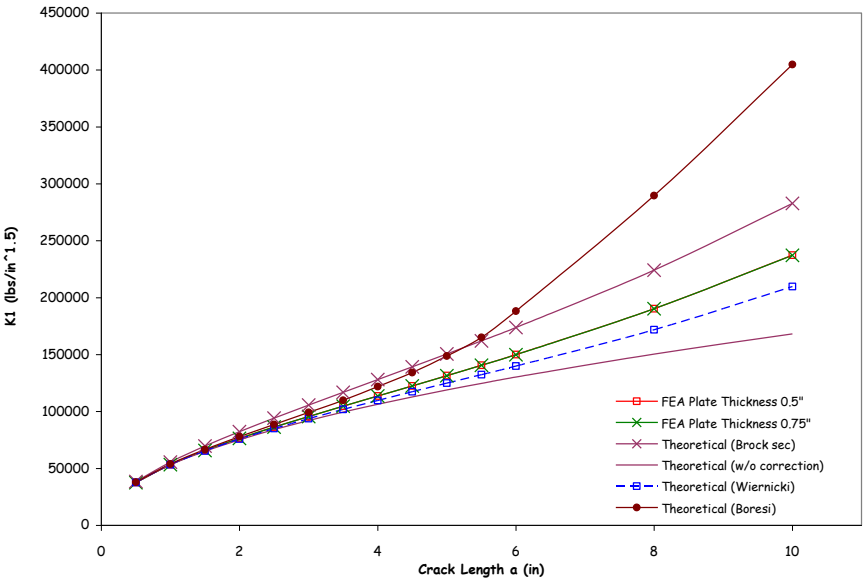


**Figure 5-4: Stress Intensity Comparison**

## 5.3 Finite Element Analysis Results – Patched Plates

The FEA model setups are summarized in Table 5-3. From each FEA model, the total force at the crack tip (sum of node forces) and the average y-displacement of the adjacent node (average nodal displacement) were extracted from the model for different crack lengths. Figure 5-5 shows a cross section through the plate with the composite patch above, the crack tip region is encircled in the figure.

**Table 5-3: Experimental Setup Summary**

| Setup | Composite Patch | Plate Thickness |
|---|---|---|
| 1 | NIL | 0.5” |
| 2 | NIL | 0.75” |
| 3 | Boron/Epoxy | 0.5” |
| 4 | Boron/Epoxy | 0.75” |
| 5 | Carbon/Epoxy | 0.5” |
| 6 | Carbon/Epoxy | 0.75” |

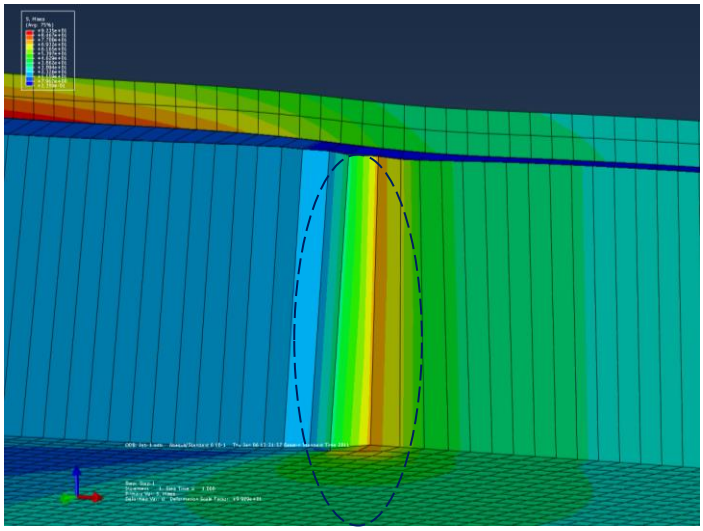

**Figure 5-5: Data Extraction Location**

The total energy release rate $G_{total}$ is calculated with the crack tip force $F_y^b$/moment $M_y^b$, adjacent node displacement $\left(u_a^y - u_y^{a'}\right)$/rotation $\left(\Psi_a^y - \Psi_y^{a'}\right)$, and distance between nodes $\Delta a$ [1] as depicted in Figure 5-6 [see for example Lena et al., Rybicki and Kanninen].

$$G_{total} = G_u + G_\Psi = \frac{1}{2\Delta a} F_y^b \left(u_a^y - u_y^{a'}\right) + \frac{1}{2\Delta a} M_x^b \left(\Psi_a^y - \Psi_y^{a'}\right) \tag{5.3}$$

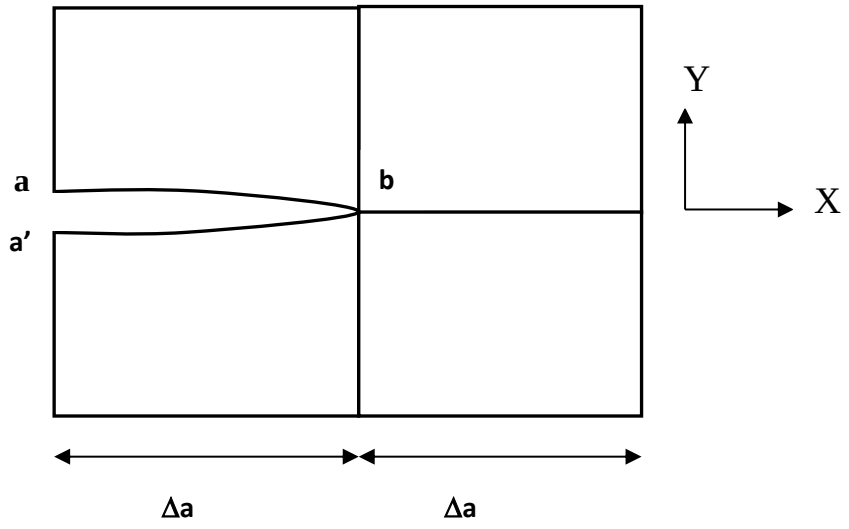


**Figure 5-6: Crack Closure Model**

[1] The nodal distance is equivalent to the element size which is 0.02in.

The FEA model uses a double patch. Hence there is no moment (rotation of the crack tip) about x-axis. Also, the nodal displacement from the FEA model is half a-a' since it uses symmetry. Hence the formula is reduced to,

$$G_{total} = G_u = \frac{F_y^b u_a^y}{\Delta a} \tag{5.4}$$

From the energy release rate G, the stress intensity factor can be calculated from equation 5:

$$K = K_u = \sqrt{\frac{G_u E_s}{t_s}} \tag{5.5}$$

where $E_s$ = Young's Modulus, $t_s$ = FEA model plate thickness.

See Figure 5-7 and Figure 5-8 for the stress intensity factor plot for both types of composite patches from the *ABAQUS* model. They are compared to Figure 5-9 and Figure 5-10, which are previous ANSYS data [Edwards and Karr,1999]. The comparisons show that both range of values and trend are similar for both FEA models. We therefore are obtaining the same results for stress intensity factors from our preliminary *ABAQUS* models as the results obtained previously using *ANSYS* software.

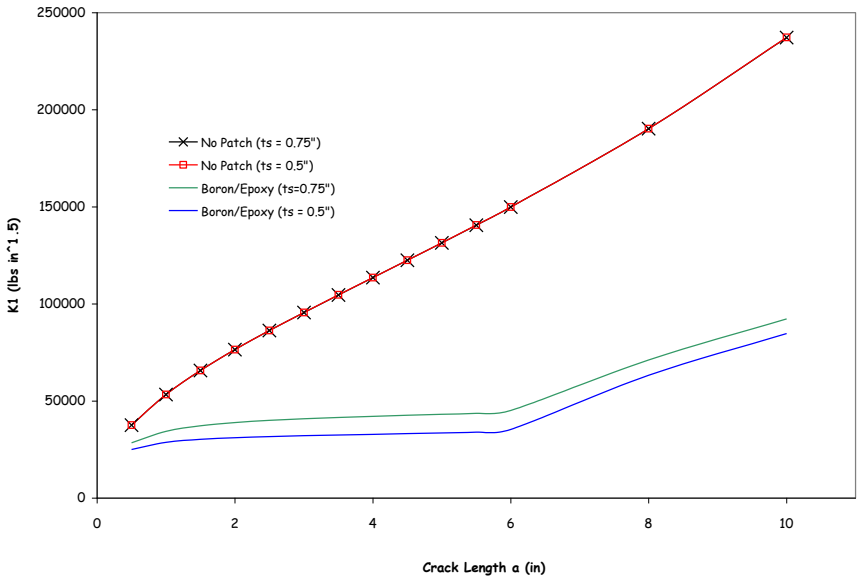


**Figure 5-7: Stress Intensity Factor Plot for Boron/Epoxy Patch**

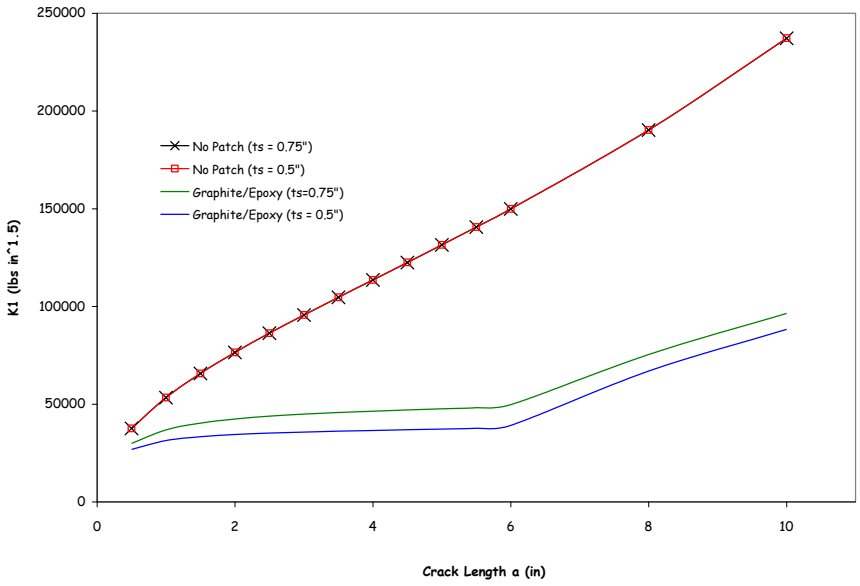


**Figure 5-8: Stress Intensity Plot for Graphite/Epoxy Patch**

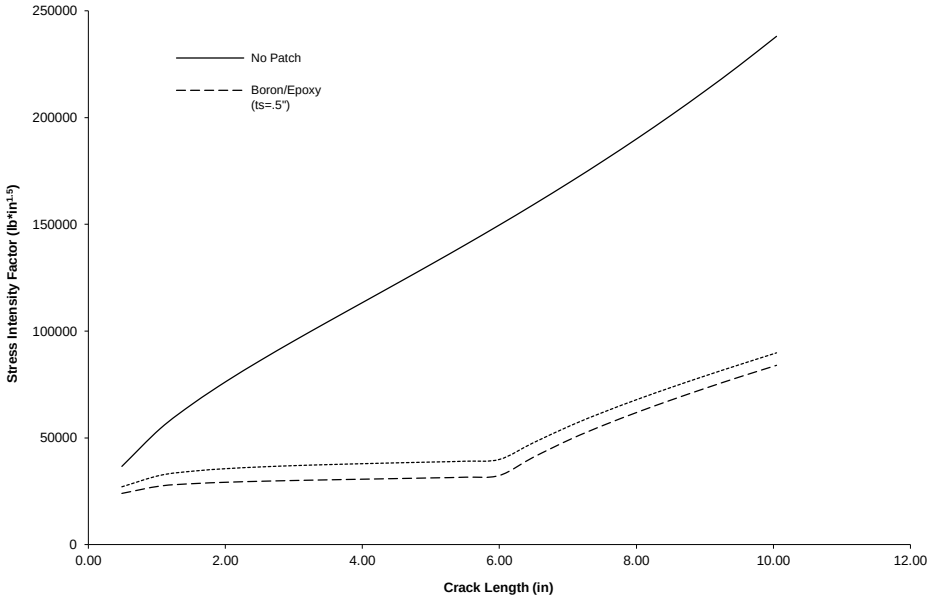


**Figure 5-9: Stress Intensity Factor Plot for Boron/Epoxy [Edwards and Karr, 1999]**

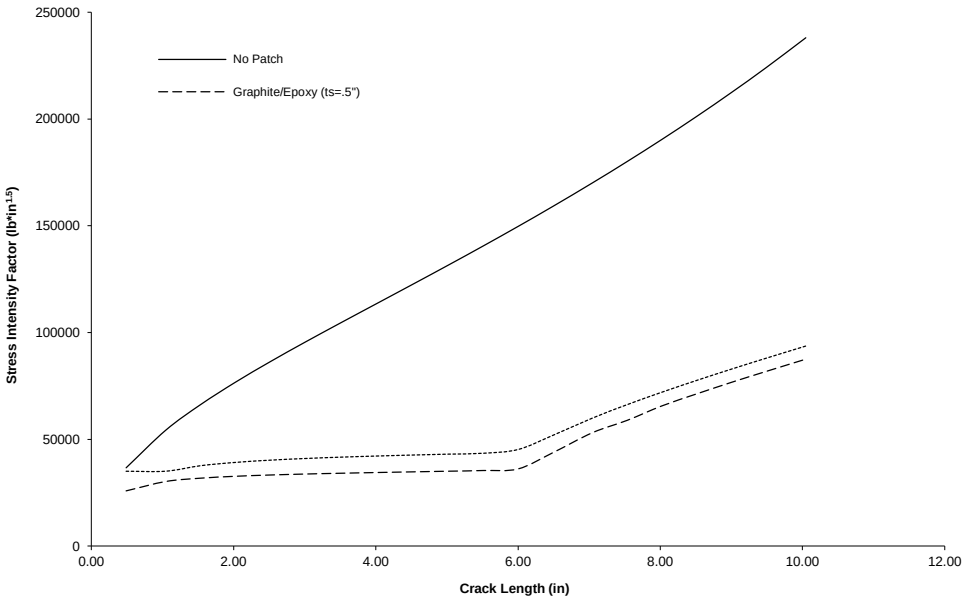


**Figure 5-10: Stress Intensity Factor Plot for Graphite/Epoxy [Edwards and Karr, 1999]**

## 5.4 Fatigue Life Calculations

The Paris Law is used to predict the fatigue life of a cracked plate [see for example Wiernicki, 1995]. This relates the stress intensity factor range based on the maximum and minimum tensile stress ($\Delta K_I$), change in crack length (da), change in the number of cycles (dN), and material properties (C and m).

$$\frac{\partial a}{\partial N} = C\left(\Delta K_I\right)^m \tag{5.6}$$

The stress intensity factor is assumed to remain constant over a small increment of crack length, $\Delta a$. The Paris law can then be discretized to determine the change in the number of cycles, $\Delta N_j$, over an interval of crack growth from $a_{j-1}$ to $a_j$ :

$$\Delta N_{a_j} = \frac{a_j - a_{j-1}}{CK^m} \tag{5.7}$$

For equation 5.7, the values of C and m are $2.3 \times 10^{-12}$ and 3.0 respectively. Units of force and length used for these values of C and m are Newton (N) and millimeter (mm) respectively. Utilizing the stress intensity factor $K_I$ found from the FEA model, the number of cycles is computed (equation 5.8) and plotted in Figure 5-11.

$$N_{a_j} = \Delta N_{a_j} + \Delta N_{a_{j-1}} + \ldots + \Delta N_{a_0} \tag{5.8}$$

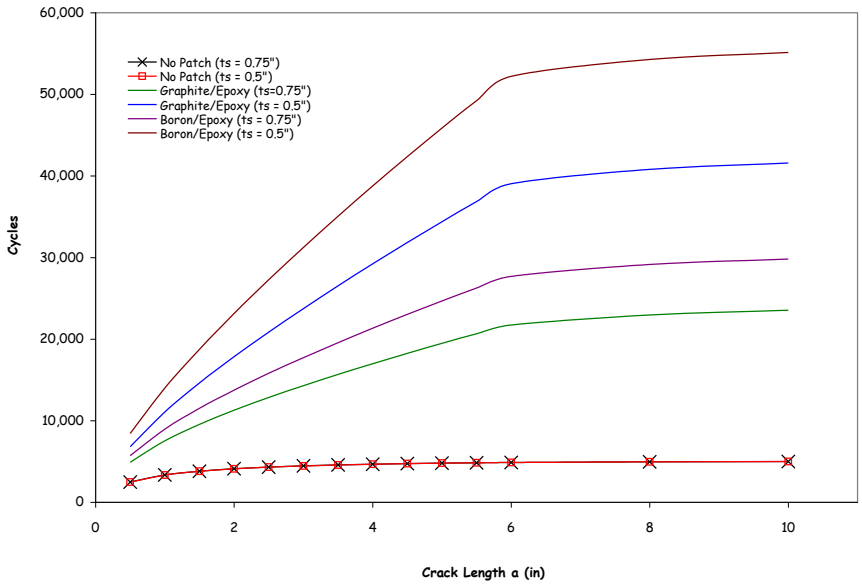


**Figure 5-11: Plot of Fatigue Life for Different Composite Patch**

The results shown in Figure 5-11 show considerable increase in fatigue life over that of the unpatched plates. The increase is on the order of a factor of 10 for most for the configuration studied here. The analysis suggests fatigue limits of upwards of 50,000 to 60,000 cycles for the composite patches.

See Appendix B for the sample calculations and Appendix C for the data used in the analyses presented in this section.

## 5.5 Further Studies of Crack Growth Predictions

Presented in section is a review of studies we conducted for the numerical analyses performed for the composite patch repair configurations. It should be noted that the results of the previous section show considerably lower fatigue life predictions than that of similar geometry analyzed by Edwards and Karr [1999]. In order to further verify our finite element models and to provide guidance for our experimental arrangements additional studies were undertaken. These studies include an analysis of double edge cracks for comparison with previous studies by Lena (1991]

### 5.5.1 Double Edge Cracks

The geometry used in the Lena paper is that of a 2024-T3 aluminum plate: length 177.8 mm (excluding the grip area), width 88.9 mm, thickness 3.175 mm. 25.4 mm cracks were seeded on either edge, and allowed to propagate towards the center. For computational efficiency, a 1/8 model was constructed, taking advantage of symmetry. The material properties and Paris' Law coefficients used in our analysis were taken from the Lena paper. As specified in the Lena paper, the loading consisted of a constant amplitude cyclic tensile load, with a peak load of 47.3 MPA.

Because an applied pressure loading was specified, in addition to generating finite element results, empirical results using the appropriate relations given by Borsei and Broek were also produced. From Borsei, the proposed geometric correction factors are given in Table 5-4

**Table 5-4: Stress Correction Factor – Double Edge Cracks**

| **λ** | **F(λ)** |
|---|---|
| 0 | 1.12 |
| 0.2 | 1.12 |
| 0.4 | 1.14 |
| 0.5 | 1.15 |
| 0.6 | 1.22 |

From Broek, the geometric correction factor was given as: $= 1.12 + 0.43\left(\frac{a}{c}\right) - 4.79(\frac{a}{c})^2 + 15.46(\frac{a}{c})^3$.

The post-processing of the numerical data was carried out as described in the previous secton. The force at the crack tip in the Y direction was measured for each crack increment, as well as the displacement in the Y direction of the adjacent node. Using this data, and making use of the modified crack closure technique, the energy release rate was calculated, which was then related to the stress intensity factor at the crack tip. Using Paris' Law, the calculated stress intensity factor was then used to calculate the fatigue life of the cracked plate. Integration of Paris' Law gives the expected fatigue life for the specimen. Note that this integral may either be solved using a separation of variables technique, such that

$$N_f = \frac{2\left(a_c^{\frac{2-m}{2}} - a_i^{\frac{2-m}{2}}\right)}{(2-m)\,C(\Delta\sigma Y\sqrt{\pi})^m} \tag{5.9}$$

or by discretization, where $\Delta N_{a_j} = \frac{a_j - a_{j-1}}{CK^m}$. The plot below, Figure 5-12, details the finite element results, as well as the empirical results and the experimental and FE results originally produced by Lena.

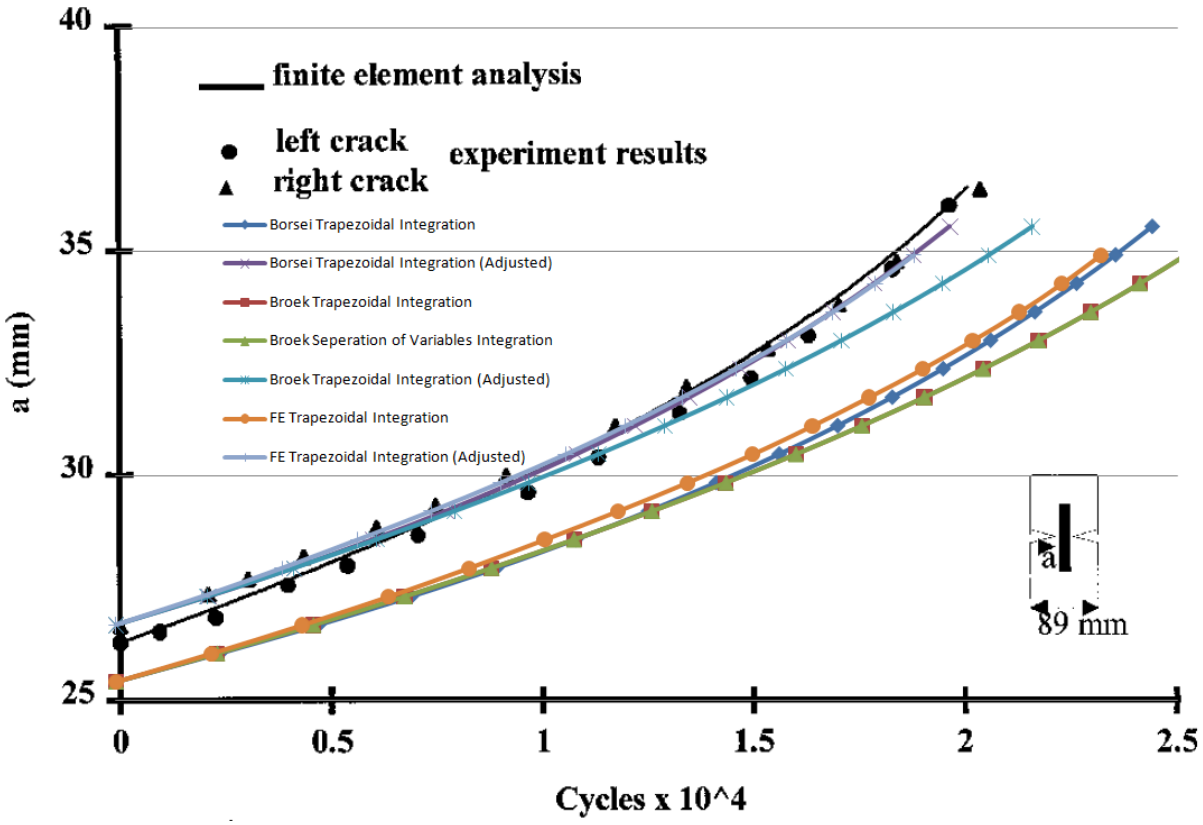


**Figure 5-12: Crack Growth Predictions for Double Edge Crack Configurations**

Inspection of the above plot shows that our data points correspond well to the finite element and experimental results obtained by Lena. Note that there is an apparent stratification in our results: the four lower results, and then the three upper 'Adjusted' lines. In the Lena paper, the experimental setup called for an initial crack length of 25.4 mm. This was the geometry that was modeled for our FE analysis, as well as using the empirical relations. Crack propagation was then simulated in 0.635 mm increments. However, inspection of the plot of the Lena results shows that the y-intercept (corresponding to zero cycles, and the initial crack length) is closer to 26.5 mm. This change in geometry alters the stress intensity factor, and in turn the solution to Paris Law integral, accounting for the disjunction between our initial results and those from Lena. The post processing of the results was then modified to assume an initial crack of 26.67 mm. These "Adjusted" results are much closer to the Lena results.

At this point, it bears mentioning the variety of techniques that may be used to integrate Paris' Law to solve for the fatigue life. As presented above, a separation of variables technique may be used. This is incumbent upon knowing $\Delta\sigma$. This method was able to be used in the Lena analysis, since an applied pressure loading along the upper and lower surfaces of the plate was specified. However, for our experiment, we must choose to either specify a uniform displacement field or a specified total force. ( The latter approach was eventually selected). A uniform state of pressure (and in turn, stress) will not be present across a section of the plate, and we will not be able to use this integration technique for comparison with our experimental results.

Alternatively, the Paris law may be simply discretized. However, care must be taken in deciding which type of quadrature to use for the numerical integration. A trapezoidal integration technique can be used, taking the $\frac{da}{dN}$ term to be the average of the terms calculated at the upper and lower bounds of the crack increment. In doing this, we are essentially averaging the K terms of the upper and lower bounds of the crack increment in question.

Below the results from the Lena validation are presented in Figure 5-13, showing 4 different integration techniques: left and right handed rectangular rules, trapezoidal, and the separation of variables. Note that the trapezoidal integration corresponds almost exactly to the separation of variables technique. Because these two results correspond, and due to the difficulty in using the separation of variables technique for our later analyses, the trapezoidal integration is the preferred post-processing method.

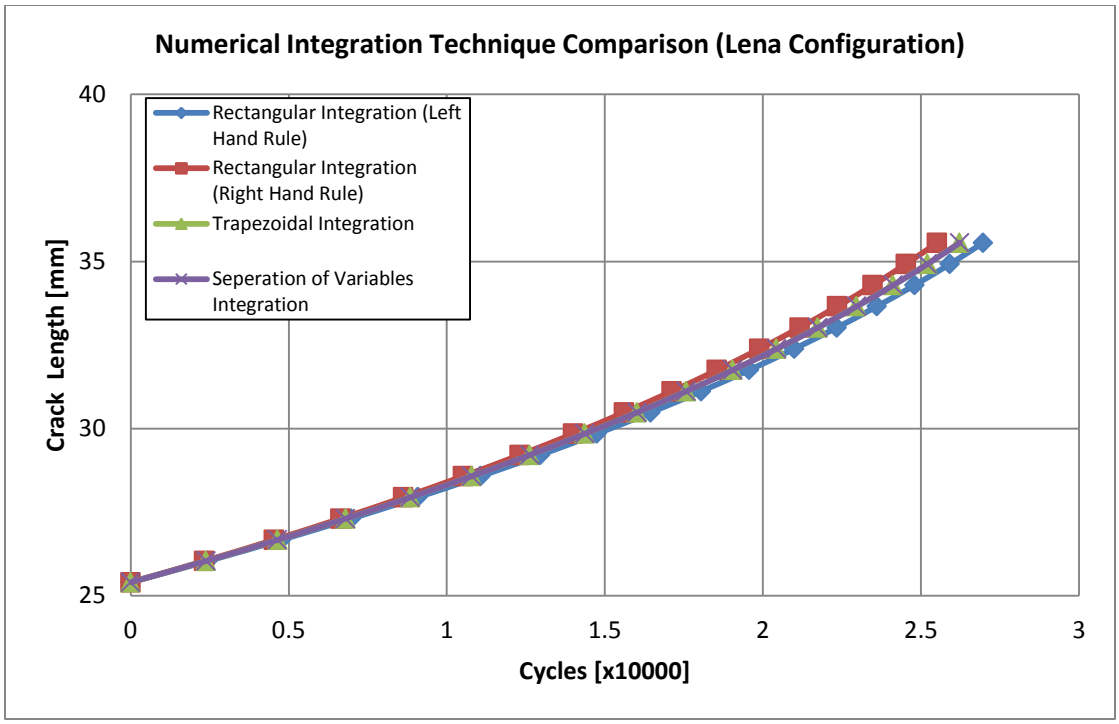


**Figure 5-13: Crack Growth Predictions for Double Edge Crack**

## 5.5.2 Single Edge Cracks

With our finite element analyses and post-processing techniques validated, and the preferred method of integration determined, it was then possible to begin the numerical analyses of our experimental design. Tentatively, our experiment was to test the fatigue properties of a 12 inch by 12 inch steel plate, with an applied 4 inch by 4 inch composite patch covering the notched edge on the top and bottom surfaces of the plate, subject to a uniform displacement field. The plate would then be cut with an edge crack, through thickness on one side of the plate.

Before evaluating this setup, it is instructive to ensure that our results again align with empirical predictions. Towards this end, a finite element model was constructed according to our proposed geometry. To validate this model, the plate was left without a patch, and a uniform pressure (as opposed to displacement) was specified on the upper and lower bounds of the plate. This setup allowed us to compare our numerical results with the predictions from Borsei and Broek, as was done for the Lena validation. For this geometry, Borsei's geometric correction factors are given Table 5-5.

**Table 5-5: Stress Correction Factor – Single Edge Cracks**

| **λ** | **F(λ)** |
|---|---|
| 0 | 1.12 |
| 0.2 | 1.37 |
| 0.4 | 2.11 |
| 0.5 | 2.83 |

From Broek, the geometric correction factor is given as: $= 1.12 + 0.23\left(\frac{a}{c}\right) + 10.56(\frac{a}{c})^2 - 21.74(\frac{a}{c})^3 + 30.42(\frac{a}{c})^4$. However, the Broek correction factor specifies that the aspect ratio of the plate must be 2; since our aspect ratio is of 1, it is not expected that the Broek factor will correspond precisely with our results.

Since Borsei only lists four values for f(λ), and linear interpolation/extrapolation of his values is not necessarily the most accurate way of determining the proper f(λ) value, a best fit fourth order polynomial was plotted through the Borsei values in an effort to improve the fidelity of the empirical result. This fourth order polynomial gives the geometric correction factor as: $f(\lambda) = 1.12 + 0.9177\left(\frac{a}{c}\right) - 0.525(\frac{a}{c})^2 + 11.083(\frac{a}{c})^3$. The fatigue life of our proposed plate, subject to a uniform pressure of 30 ksi is shown below in Figure 5-14. Note the close correlation of the FE result with the fourth order approximation of Borsei, as well as the decided overestimation from Broek (undoubtedly due to the discrepancy in plate aspect ratio).

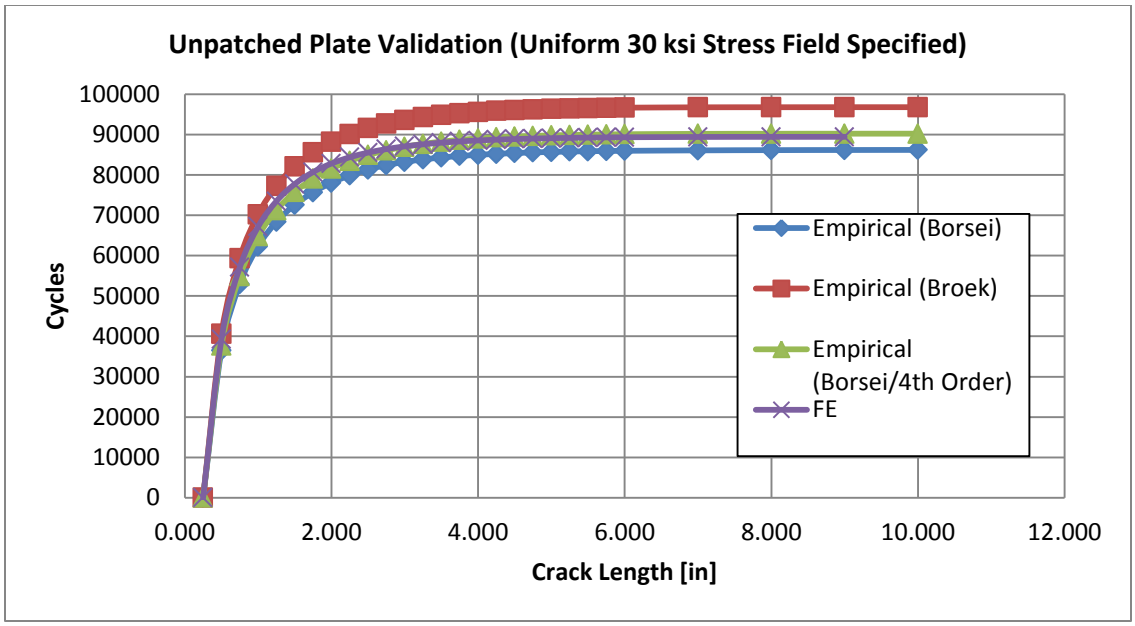


**Figure 5-14: Fatigue Life for An Unpatched plate with a Single Edge Crack**

With the FE model for our experimental design validated, it was now possible to specify a displacement field instead of an applied pressure at the upper and lower surfaces. For an unpatched plate we assume again C and m are taken as $2.3x10^{-12}$ and 3.0, respectively. Results are shown below in Figure 5-15.

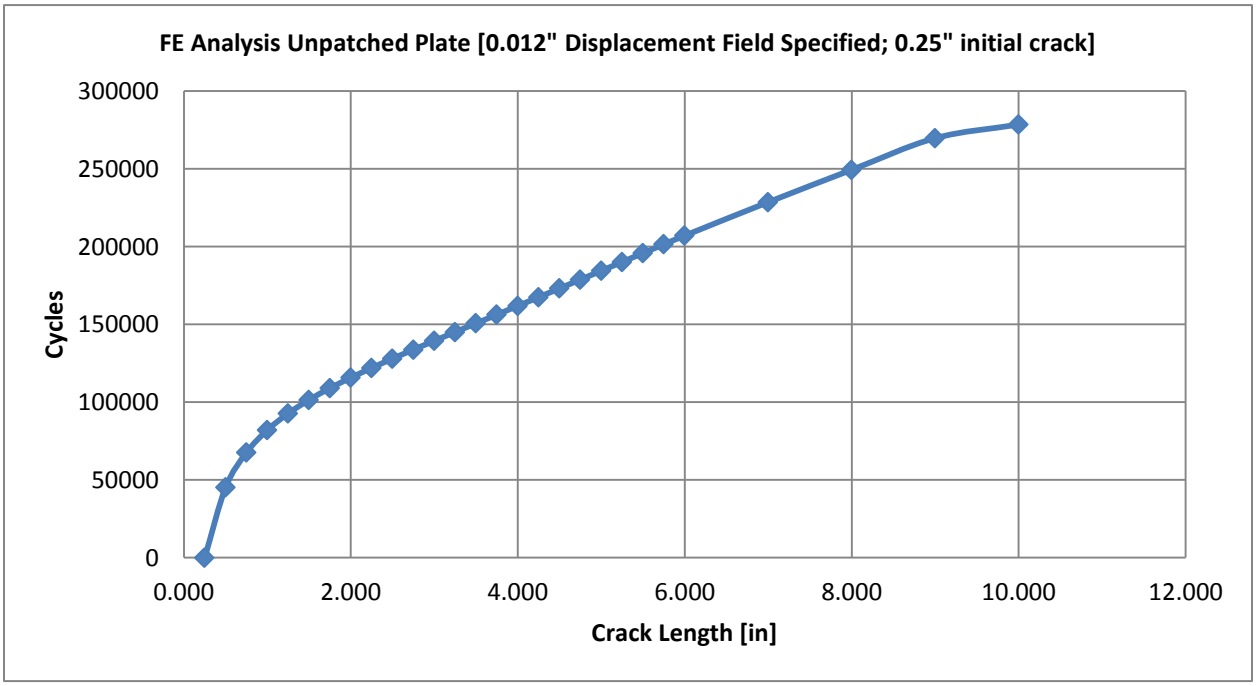


**Figure 5-15: Fatigue Life for Different Composite Patches**

Note that it is thus predicted to take about 280,000 cycles for the crack to propagate from 0.25 inches to 10 inches when a displacement field of 0.012 inches is specified. For our material properties and geometry, this displacement would initially correspond to a pressure field of about 30 ksi, assuming an intact, crack free plate ($\Delta = \frac{PL}{AE}$). Compare these 280,000 cycles to the 90,000 cycles for the same extent of crack propagation when the pressure field was specified at 30 ksi. The difference in the fatigue lives when comparing a plate subject to a uniform displacement field and uniform pressure field is considerable, roughly a factor of 3. This is explained by the fact that while the pressure field would be similar when the crack is small, as the crack grows, the force (or pressure) needed to reach the specified displacement is less. For example, when the crack is halfway through the plate, it follows that only one half of the initial force required to displace the plate would now be necessary.

With results obtained for an unpatched plate, it was now possible to add the patch and adhesive layers in ABAQUS, and obtain results for the patched configuration. For these cases, a boron patch was used, since the boron/epoxy composite has a higher Young's modulus, and is expected to extend the fatigue life to the greatest degree (and thus pose the limiting scenario for our actual testing). Results for the plate in the patched condition are provided below. As well, the results are presented in tabular form. Figure 5-16 is for C and m values of 2.3 $x10^{-12}$ and 3.0, respectively, while the second plot, Figure 5-17, is for values of $1.0x10^{-11}$ and 3.0.

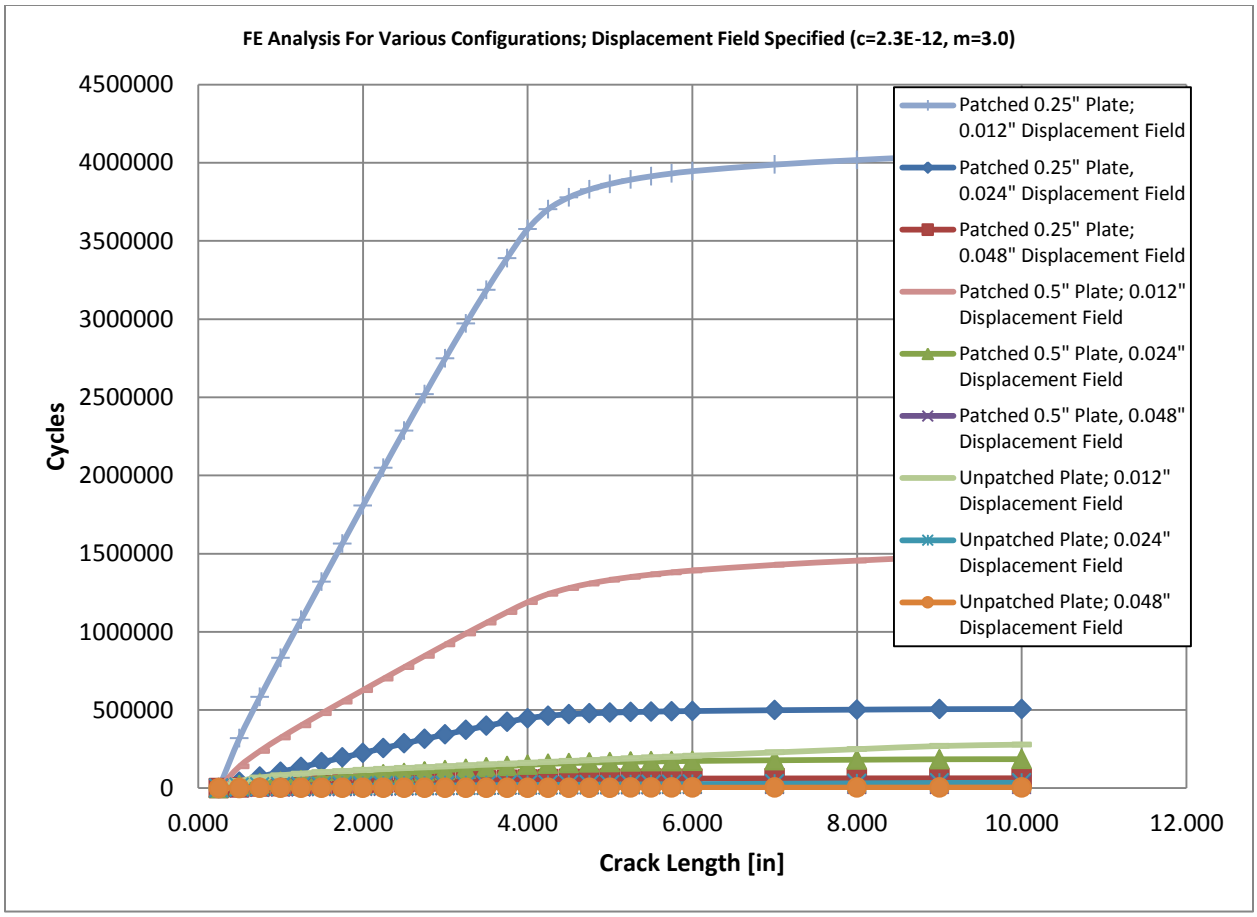


**Figure 5-16: Fatigue Life Predictions for Different Composite Patches (c=2.3E-12)**

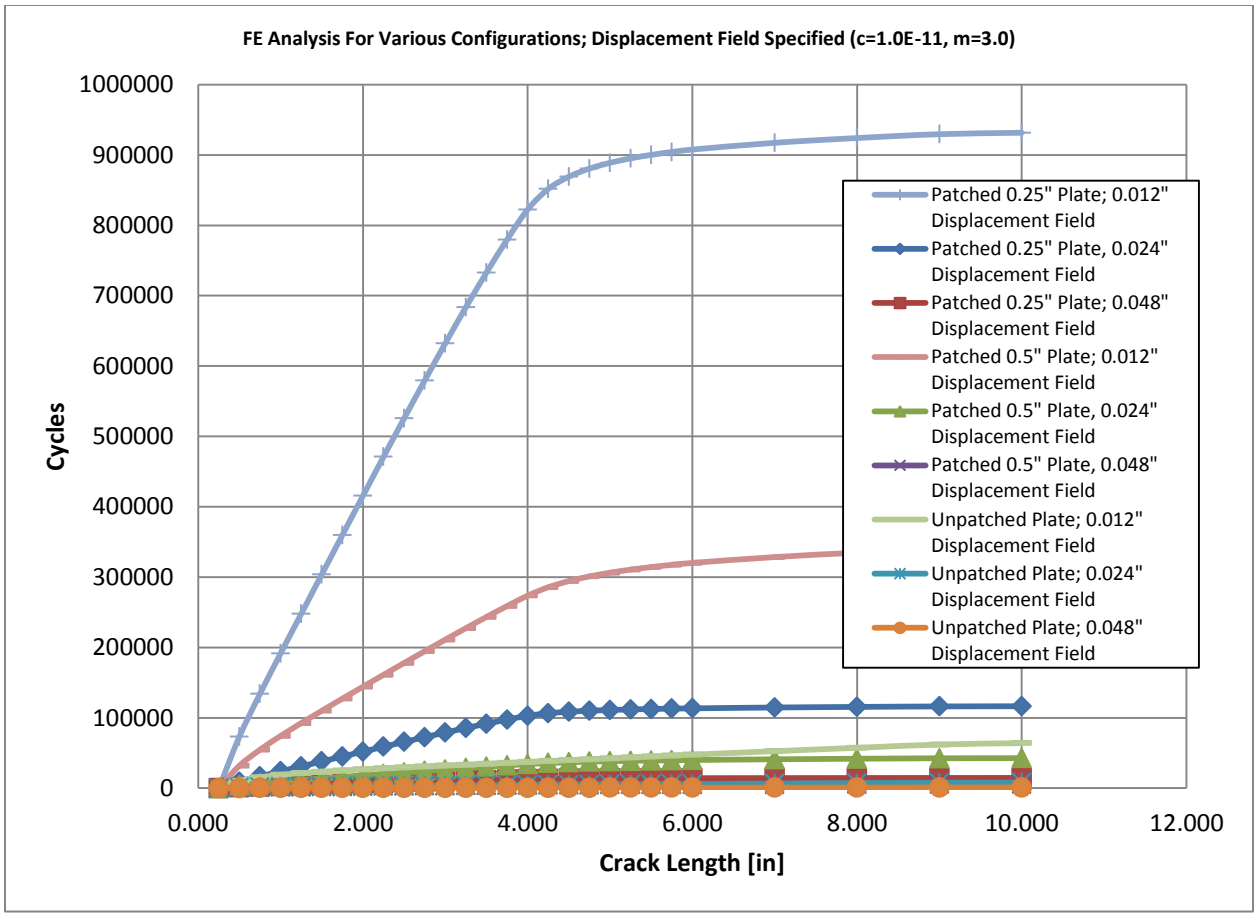


**Figure 5-17: Fatigue Life for Different Composite Patches (c=21.0E-11)**

Another consideration as planned for experimental work is the duration of the experiments in terms of number of cycles and elapsed time. There are of course mechanical limitations to frequency based on the Instron machine. As well, we must be mindful of the inherent energy dissipation considerations, and try to minimize specimen heating, which would alter the stress at the crack tip, and our results as well. For low cycle fatigue testing (10-$10^5$ cycles), cyclic frequency is usually on the order of 1 to 2 Hz.

# 6. Fatigue Testing Results

Based on the finite element results and the types of fracture problems faced in practice, we decided to use the facilities at the University of Michigan's Structural Engineering Laboratory, directed by Professor Gustavo J. Parra-Montesinos. This allowed for the use of thicker steel plating (1/4 in.) than the facilities at the Composite Materials Laboratory (as was originally proposed) could accommodate. The structural steel plating was then pre-cut with a single side crack of 3 inches in length. This would allow for reasonable levels of forcing as well as accomplishing the tests within a reasonable amount of cycles and time. In addition the testing machine's cycling loading capacity and programming was conducive to prescribed cyclic force levels.

Tests were conducted on several steel plates to experimentally validate the effectiveness of using composite patches as a means to prevent crack growth and extend the fatigue life of structural components. Specimens were tested with and without the use of reinforcements in order to corroborate the analyses. New finite element models were then developed again using the commercial software *ABAQUS*.

## 6.1 Procedure

Two configurations were investigated. Steel plates having a length of 18.0 in, a width of 12.0 in, and a thickness of 0.25 in, with a 3.0 inches initial crack at mid span were first studied without the use of reinforcements. Other plates of similar geometry were then examined using symmetric reinforcements (double-sided). All specimens were tested using a load frame manufactured by Instron (serial number: UK o28). A cyclic tensional load oscillating between 2.0 and 50.0 kips was applied at one end of the plates. Plates were pinned connected at the top and bottom; restricting both vertical and horizontal displacements but rotations about the pins were not restricted. Thus our boundary conditions are somewhat different than those used in the preliminary finite element analyses.

All composite patches were cut forming a 5.0 by 5.0 inch square, having a thickness of 1/16 inches. They were placed directly on top of the initial crack on both sides of the plates. They were then attached to the steel plates using Loctite Hysol 9340 epoxy. In order for the epoxy to achieve maximum strength, a curing process was necessary. Full cure time was 24 hours at 77˚F as instructed by its manufacturer. It was decided to use epoxy with room temperature cure because that would be the easiest method in practice although more elaborate curing methods often provide better bonding traits.

The epoxy was applied to both the patch and the plate and was evenly spread throughout, covering both surfaces entirely. Once the patch was placed on one side of the plate, weight was carefully set on top in order to remove any air bubbles, and ensure that members were completely attached. A 24-hour period passed before the other side of the plate was addressed, since as previously mentioned, full cure occurred after 24 hours at a room temperature of 77˚F.

Front and side profiles drawn to scale are presented in Figures 6-1 and 6-2.

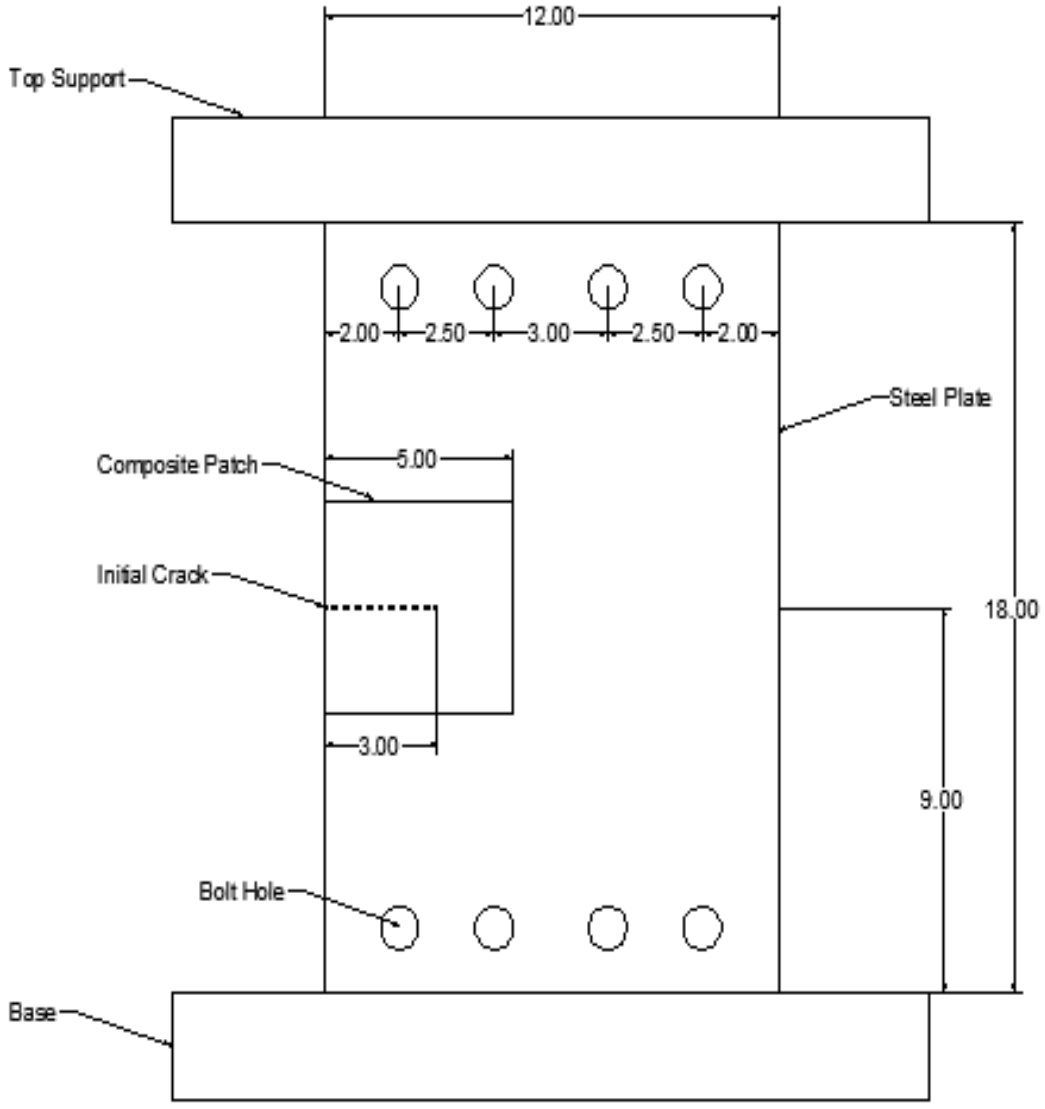


**Figure 6-1**. Specimen Front View

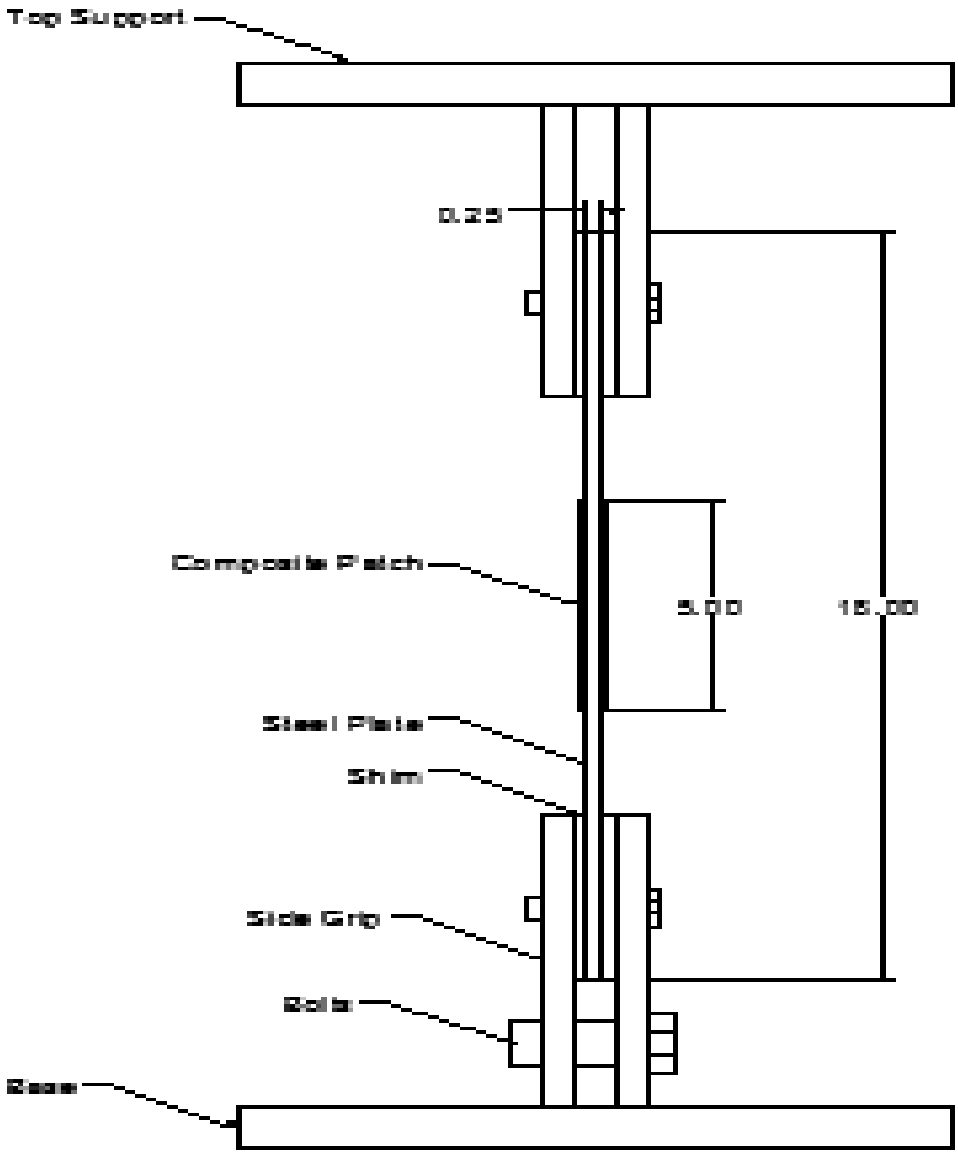


**Figure 6-2.** Specimen side view

Data were collected using an Optotrak camera system. Sensors (markers) were attached directly on one side of the plate. These markers were positioned throughout the surface of the plate as Figure 4 shows. The markers' displacements were measured and captured by the camera and the information was stored in Excel files. Data was collected at a frequency of 20.0 Hertz. The location of the markers varied between tests. One of the configurations used is shown on the figure below.

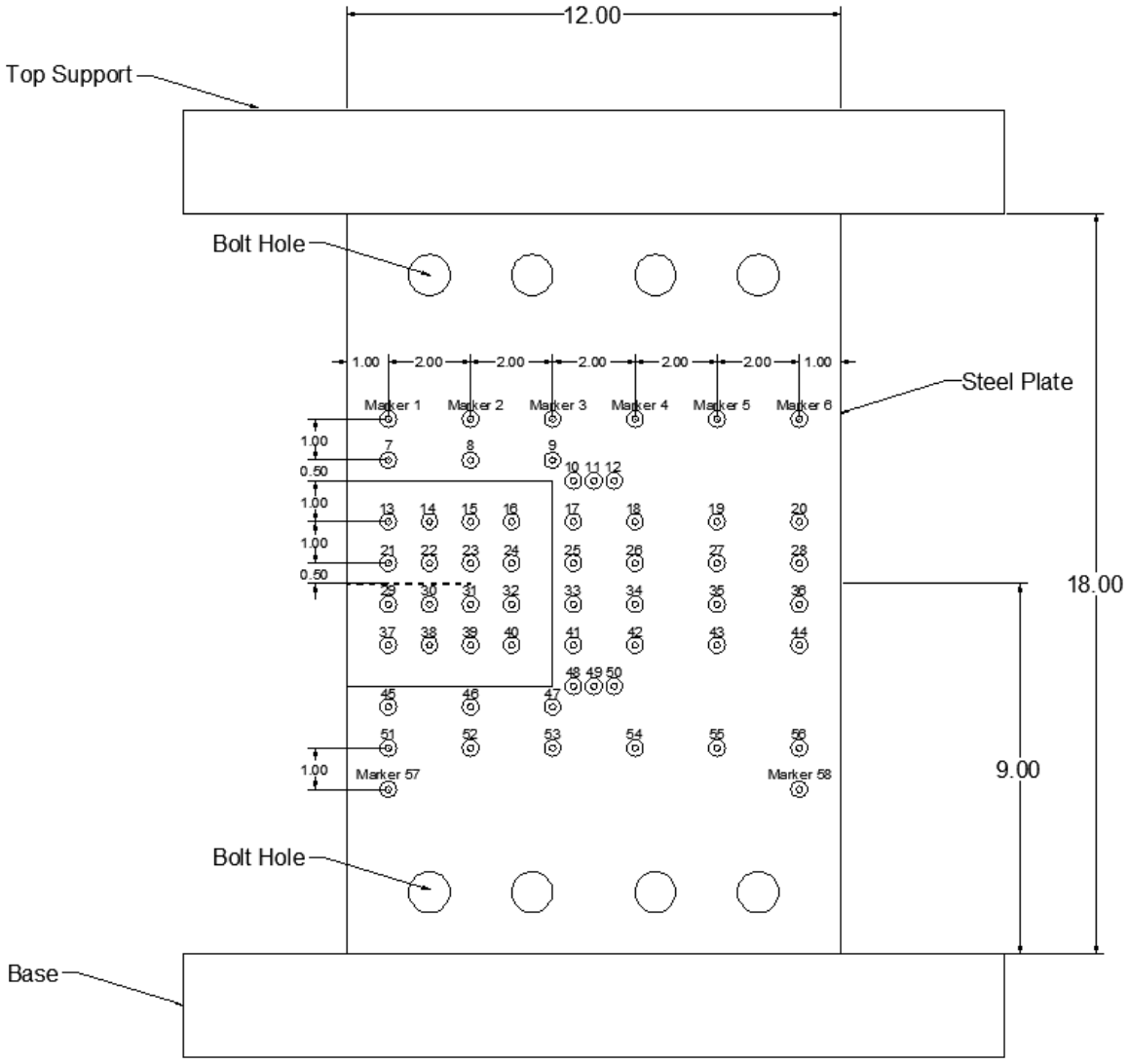


**Figure 6-3.** Specimen showing Optotrak marker locations

## 6.2 Material Property Testing

Material properties of this steel were determined experimentally. Three samples were extracted for analysis from one random plate. Stress-Strain diagrams were obtained for all three samples. The ultimate stress, yield strength, and modulus of elasticity were determined from these plots. Figures 6.4, 6.5 and 6.6 show the stress-strain diagrams for the three steel specimens tested. Results are provided below in Table 6-1.

**Table 6-1 Material Properties Of Steel Plating**

| | **Modulus of Elasticity (ksi)** | **Yield Strength (ksi)** | **Ultimate Stress (ksi)** |
|---|---|---|---|
| | | | |
| Sample #1 | 30.9 | 65.6 | 75.5 |
| Sample #2 | 31.3 | 64.6 | 75.1 |
| Sample #3 | 31.1 | 65.7 | 74.8 |

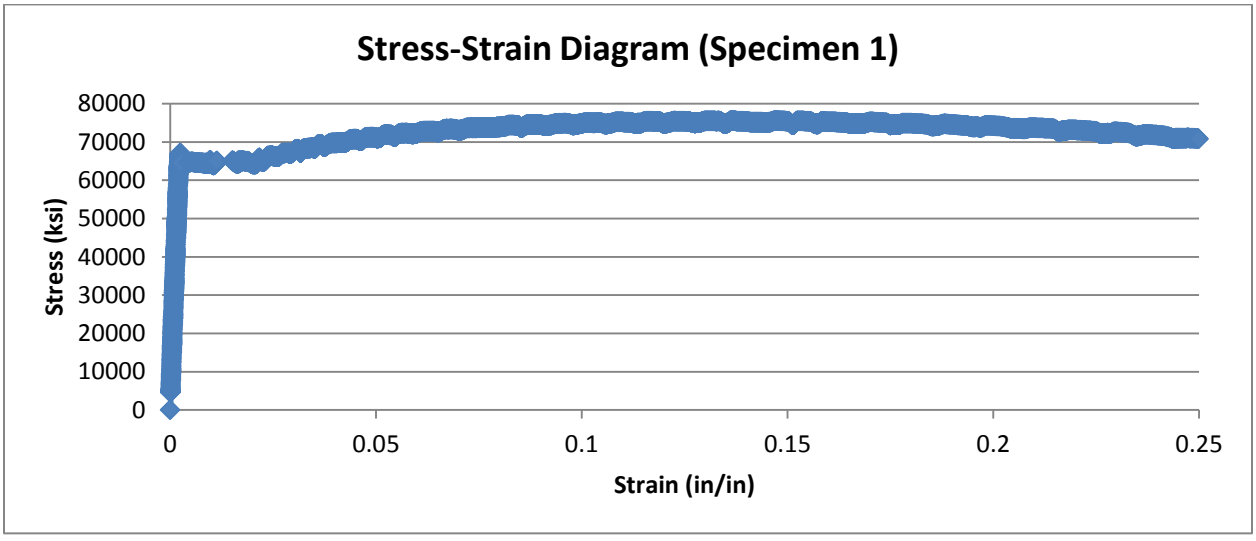


**Figure 6-4.** Stress-strain diagram from steel sample 1

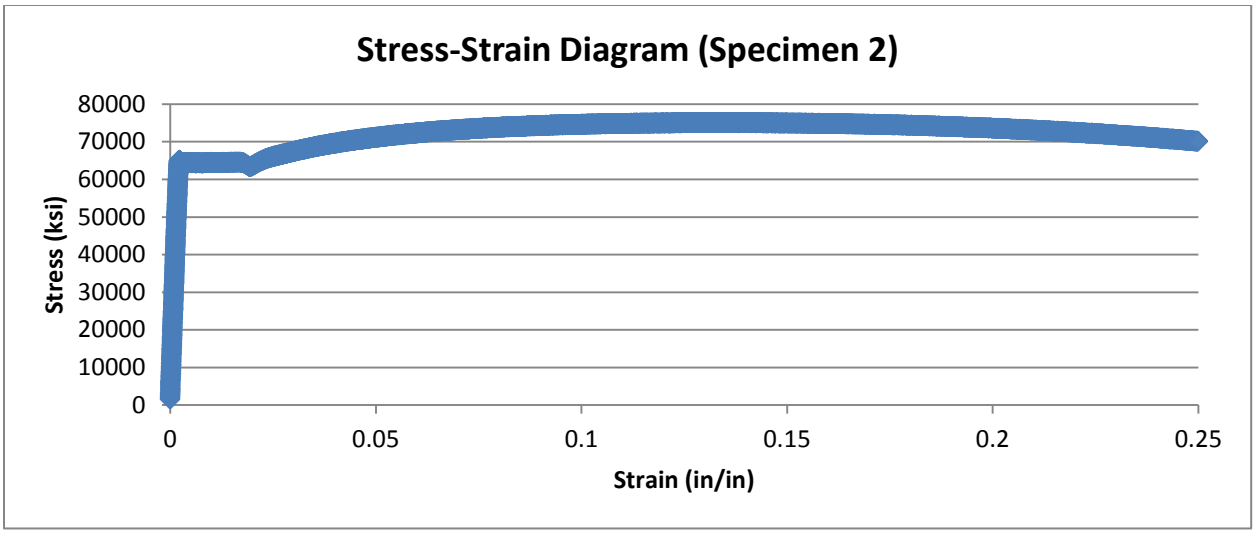


**Figure 6-5.** Stress-strain diagram from steel sample 2

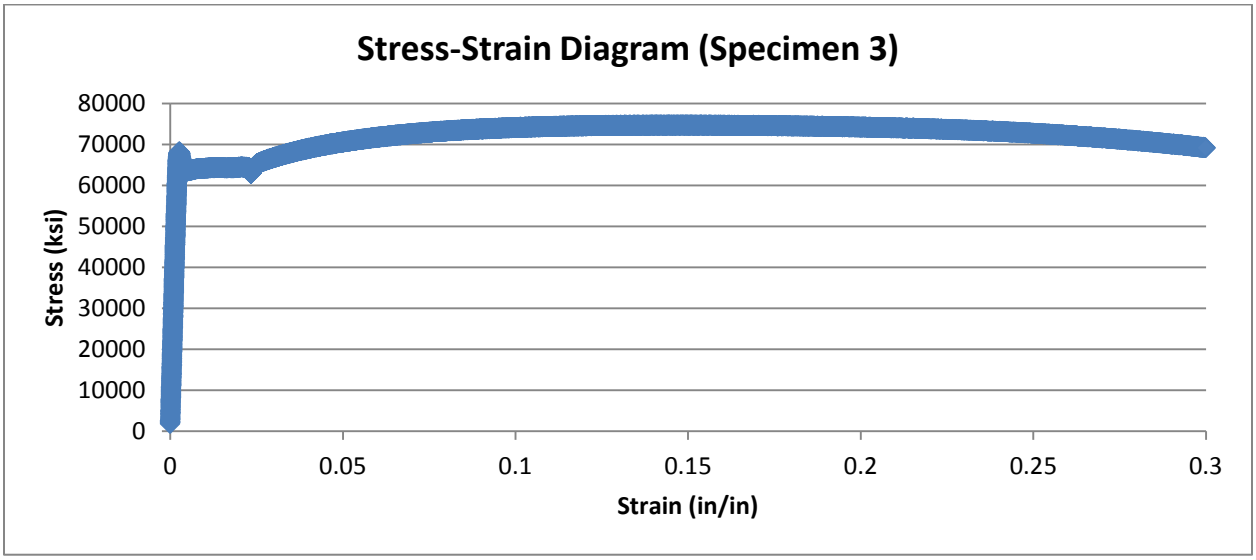


**Figure 6-6.** Stress-strain diagram from steel sample #3

Two types of composite patches were tested in this experiment; a high-strength flexible carbon fiber and a high-strength rigid carbon fiber. Material properties of these carbon fibers were determined experimentally. A total of four samples (two of each type) were tested. Stress-strain diagrams were generated for all samples in order to determine these properties. Figures 6-7 to 6-10 show the stress-strain diagram obtained for the rigid patch samples. Material properties are given on Table 6-2.

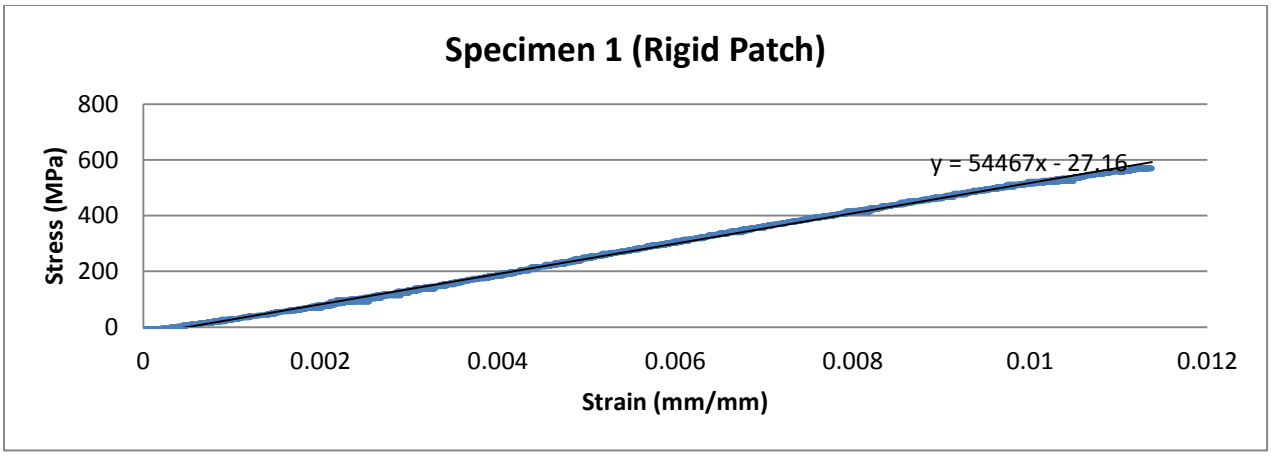


**Figure 6-7.** Stress-strain diagram for rigid patch sample #1

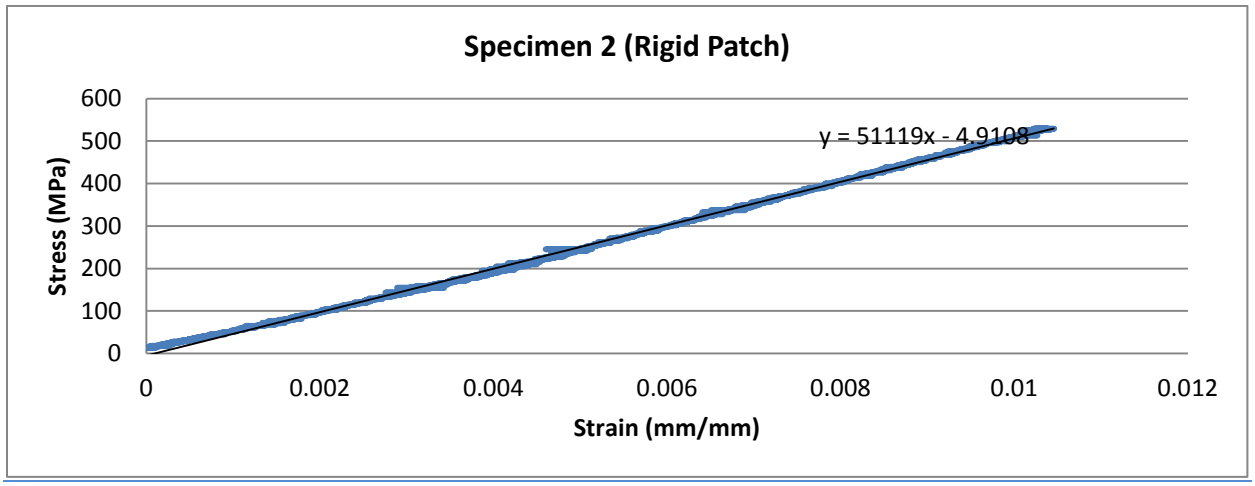


**Figure 6-8.** Stress-strain diagram from patch sample #2

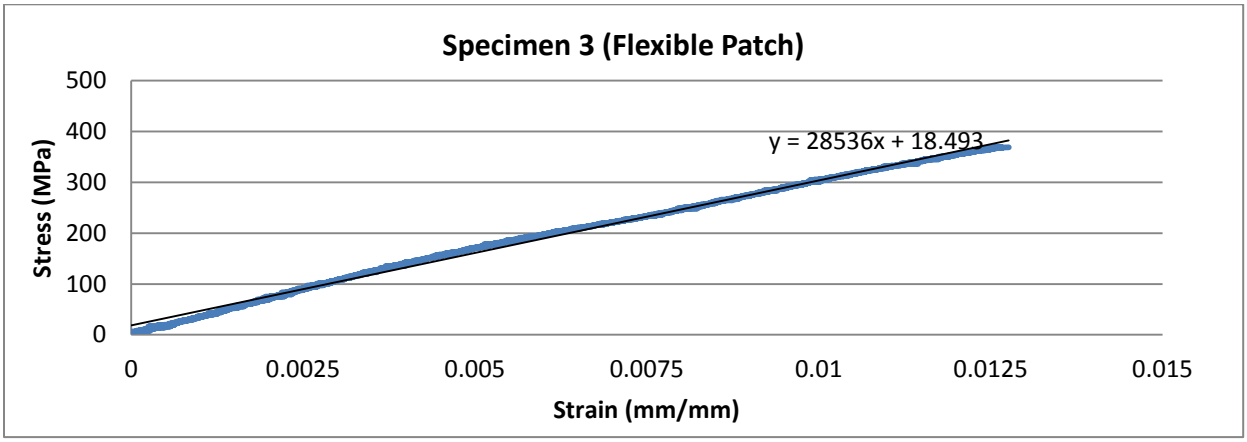


**Figure 6-9.** Stress-strain diagram from flexible patch sample #3

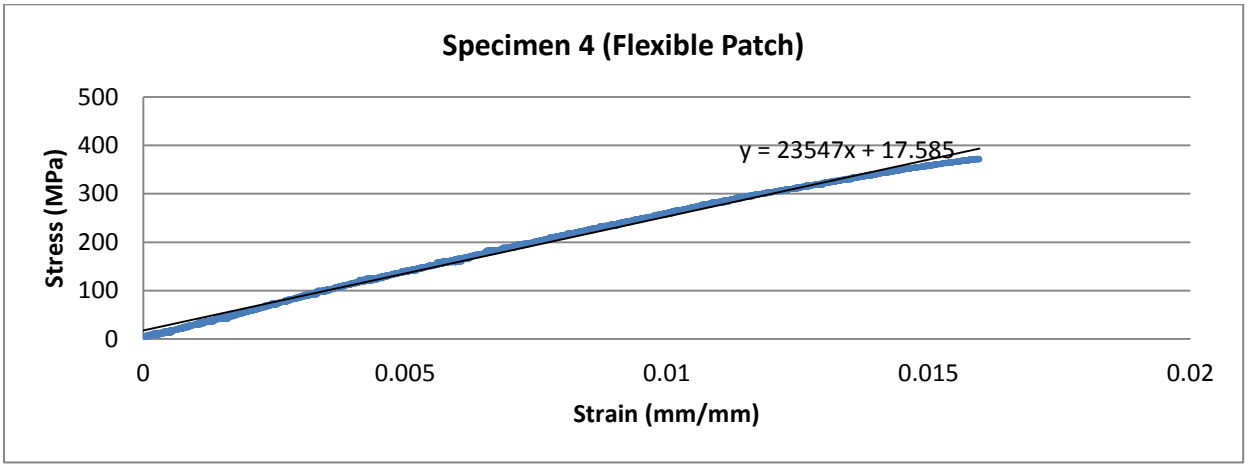


**Figure 6-10.** Stress-strain diagram from flexible patch sample #4

**Table 6-2.** Material properties of the composite patches used during testing

| **Specimen #** | **Young's Modulus (MPa)** | **Young's Modulus (ksi)** |
|---|---|---|
| | | |
| 1 (Rigid) | 54,667 | 7,899.8 |
| 2 (Rigid) | 51,119 | 7,414.2 |
| 3 (Flexible) | 28,536 | 4,138.8 |
| 4 (Flexible) | 23,547 | 3,415.2 |

## 6.3 Fatigue Test Setup

Data collected using the Optotrak camera system was used to determine the relative displacements between markers symmetrically positioned about the plate's midspan. With this information, one can determine how the crack propagates in the vertical direction as a function of the number of cycles. As an example, the marker locations for our first unpatched test is shown in Figure 6-11. Shown in Figures 6-12 to 6-14 are photographs of the test setup.

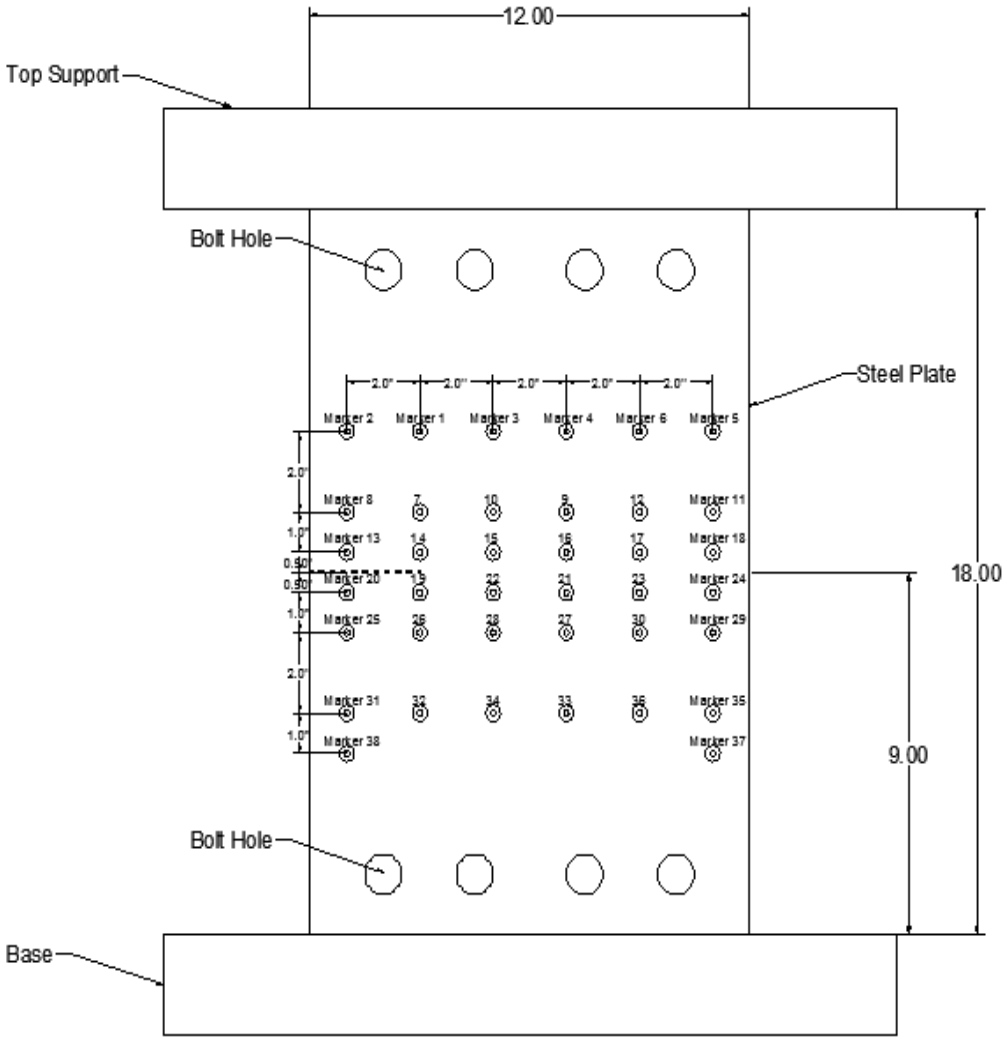


**Figure 6-11.** Unpatched Plate Marker Locations

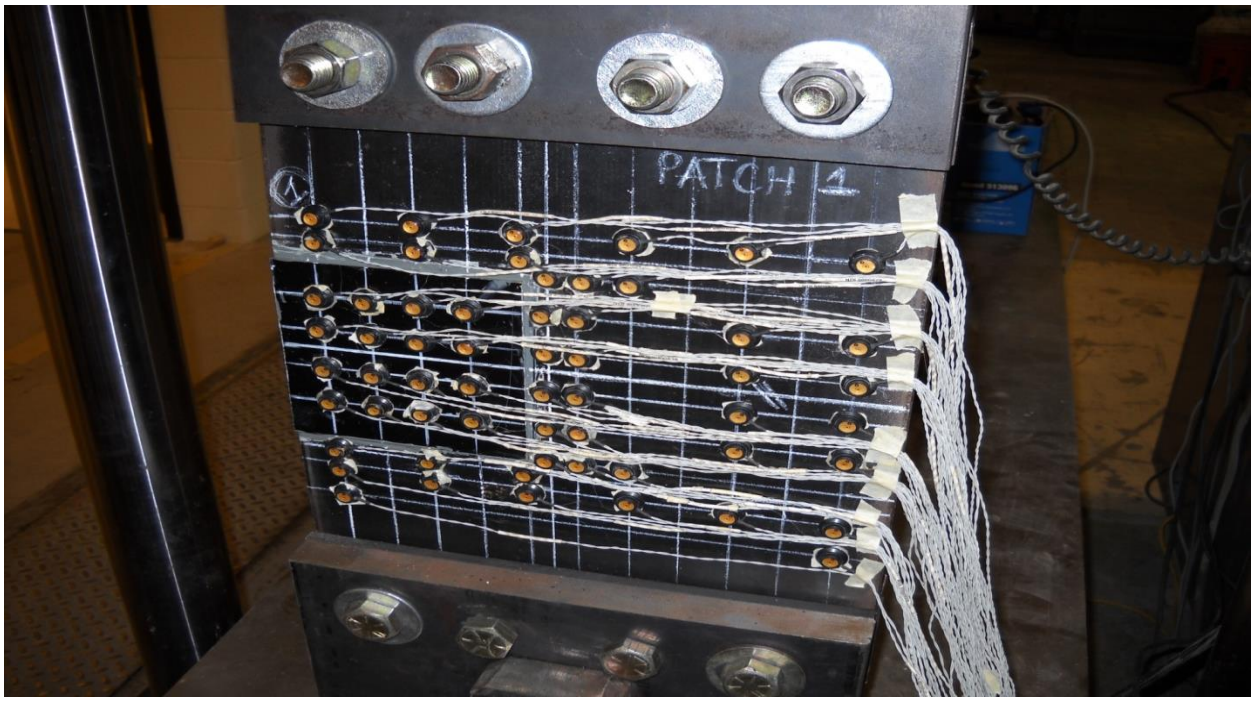


**Figure 6-12.** Front view of the plate with a flexible patch and location of markers

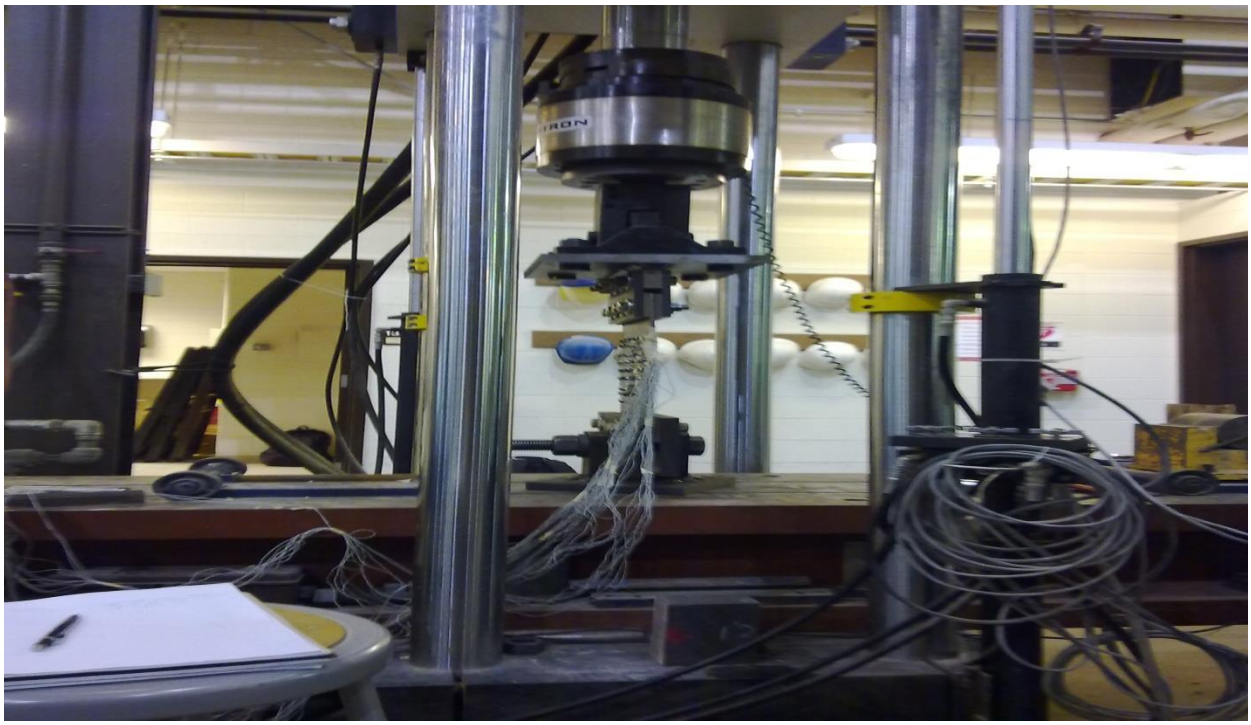

**Figure 6-13.** Specimen side view and load cell used for testing

**Figure 6-14.** Back view of specimen

## 6.4 Finite Element Modeling

The finite element software Abaqus/CAE version 6.1.1 was used to model the crack propagation for both the unpatched and patched plate configurations. To simplify the analysis a half model was used in which the experimental setup was assumed to have symmetry about the central horizontal axis.

Again using Paris' law, as described in the previous sections, this modeling was done for the bare steel plate as well as for a plate which has been patched with the graphite patches on both sides of the plate, attached with epoxy adhesive. The results from this modeling were then compared to the Boresi and Broek methods of calculating crack propagation as well as the results of the experimental tests.

Four materials were used in the various plate configurations. The properties of these materials are given in Table 6-3. This data was used to determine the propagation of the crack as a function of the cycle number. The sizes of each part used in the finite element model are given in Table 6-4. The mesh sizes through each of the thicknesses for each element are given in Table 6-5.

**Table 6-3: Material Properties**

| Material | Modulus of Elasticity [N/mm$^2$] | Poisson's Ratio |
|---|---|---|
| ASTM-A36 Steel | 2.07E+05 | 0.30 |
| Epoxy Adhesive | 1.93E+03 | 0.27 |
| Graphite/Epoxy Composite | 2.60E+04 | 0.30 |
| Boron/Epoxy Composite | 5.28E+04 | 0.30 |

**Table 6-4: Part Dimensions**

| Part | X Dimension [1n] | Y Dimension [1n] | Z Dimension [1n] |
|---|---|---|---|
| Steel Plate | 12.00 | 6.00 | 0.2500 |
| Rigid Top | 12.00 | 6.00 | 0.2500 |
| Epoxy Adhesive | 5.00 | 2.50 | 0.0315 |
| Composite Patch | 5.00 | 2.50 | 0.0625 |

**Table 6-5: Mesh Sizes**

| Part | X Spacing [-] | Y Spacing [-] | Z Spacing [-] |
|---|---|---|---|
| Steel Plate | 0.05 | 0.05 | 0.0625 |
| Rigid Top | 0.05 | 1.20 | 0.0625 |
| Epoxy Adhesive | 0.05 | 0.05 | 0.0315 |
| Composite Patch | 0.05 | 0.05 | 0.03125 |

The model assemblies are shown in Figure 6-15. Note the Epoxy Adhesive and Composite Patch on the negative Z side of the steel plate are not visible in this figure.

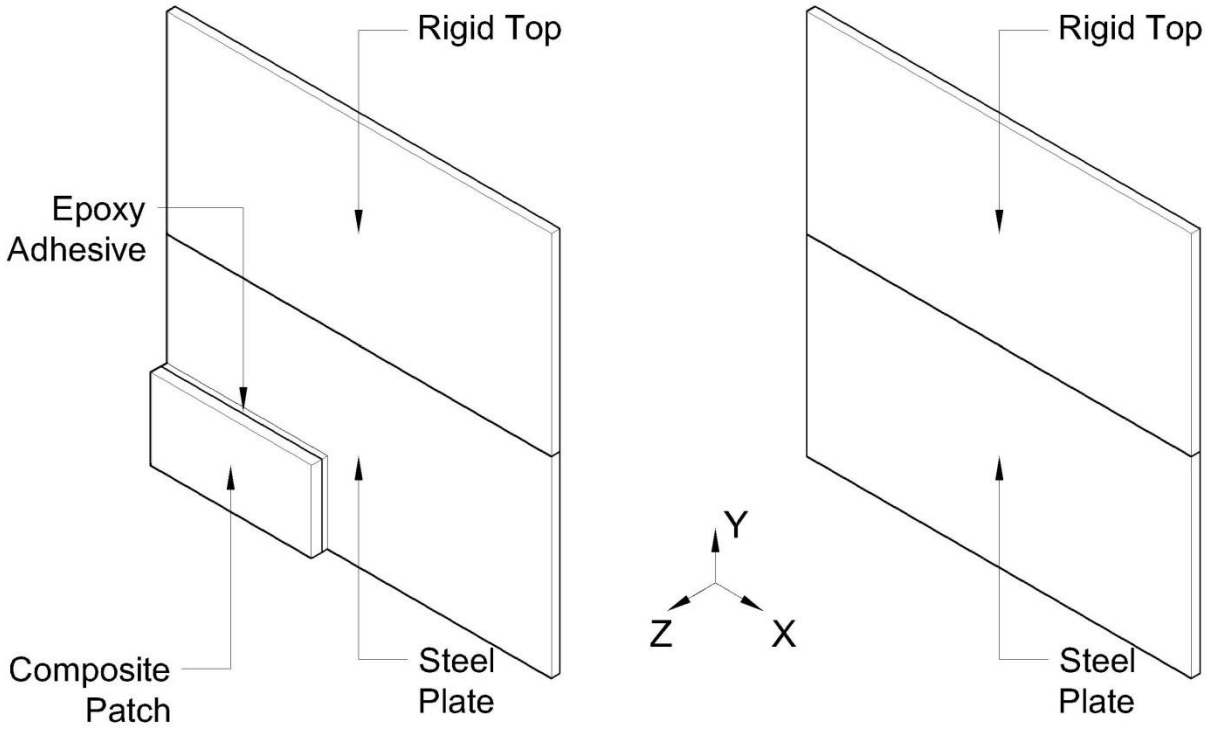


**Figure 6-15: Model Assembly**

The adjacent surfaces of each part must be constrained to allow for the proper interactions. Finally, the material properties of each part must be selected, as given in Table 6-6. These properties are selected for elastic materials.

**Table 6-6: Finite Element Model Material Properties**

| Material | Modulus of Elasticity [psi] | Poisson's Ratio [-] |
|---|---|---|
| Steel Plate | 30,000,000 | 0.35 |
| Epoxy Adhesive | 280,000 | 0.27 |
| Graphite/Epoxy Composite | 3,777,188 | 0.30 |
| Boron/Epoxy Composite | 7,657,359 | 0.30 |
| Rigid Top | 9,999,999,000 | 0.01 |

The next step in the finite element model analysis is to create the loading and boundary conditions. These conditions are somewhat different than the previous analyses which used prescribed far-field displacements and uniform stresses. The test conditions are depicted in Figure 6-16.

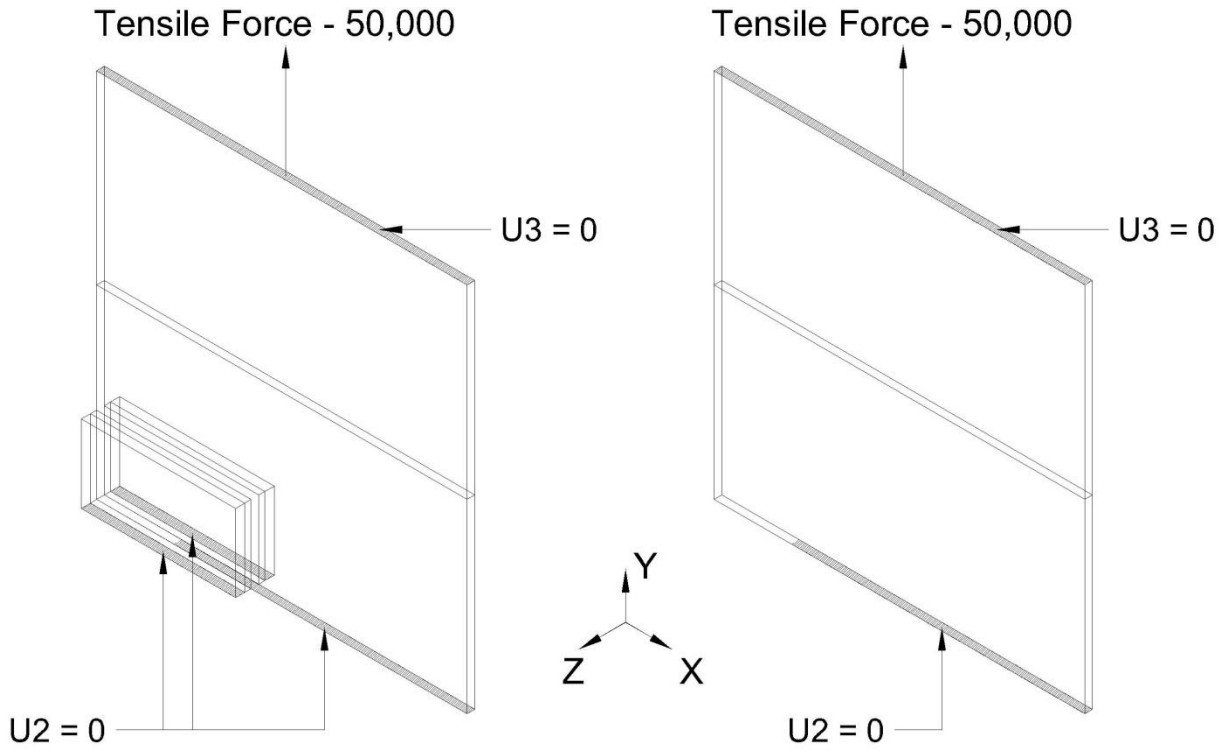


**Figure 6-16: Boundary Conditions and Loading ( the units of Force are in pounds).**

The FEA results of crack propagation of plate with and without patch can be obtained after following the step by step procedures described in previous sections. The finite element analysis results of crack propagation of unpatched plate with an initial edge crack length of 3.0 inches are shown in Figure 6-17. In addition to the finite element results, empirical methods were used to display the crack propagation as a comparison with the finite element results. The experimental results, together with the FEA as well as the first unpatched test results are also shown. This shows that there is little difference between the FEA and experimental results, implying that the finite element modeling is effective and the results are reliable. The C and m parameters in the Paris Law are also approximated accurately. Based on the results above, it could be concluded that FEA and Boresi methods are effective in modeling the crack propagation of unpatched plate.

The finite element analysis results of crack propagation of patched plate with an initial edge crack length of 3.0 inches are shown in Figure 6-17. Two kinds of composite patches, the Graphite rigid and flexible plates, are studied. The FEA results imply an increase in fatigue life

of nearly two orders of magnitude. As discussed in the following section, our test results however shown approximately an order of magnitude increase rather than two orders of magnitude increase.

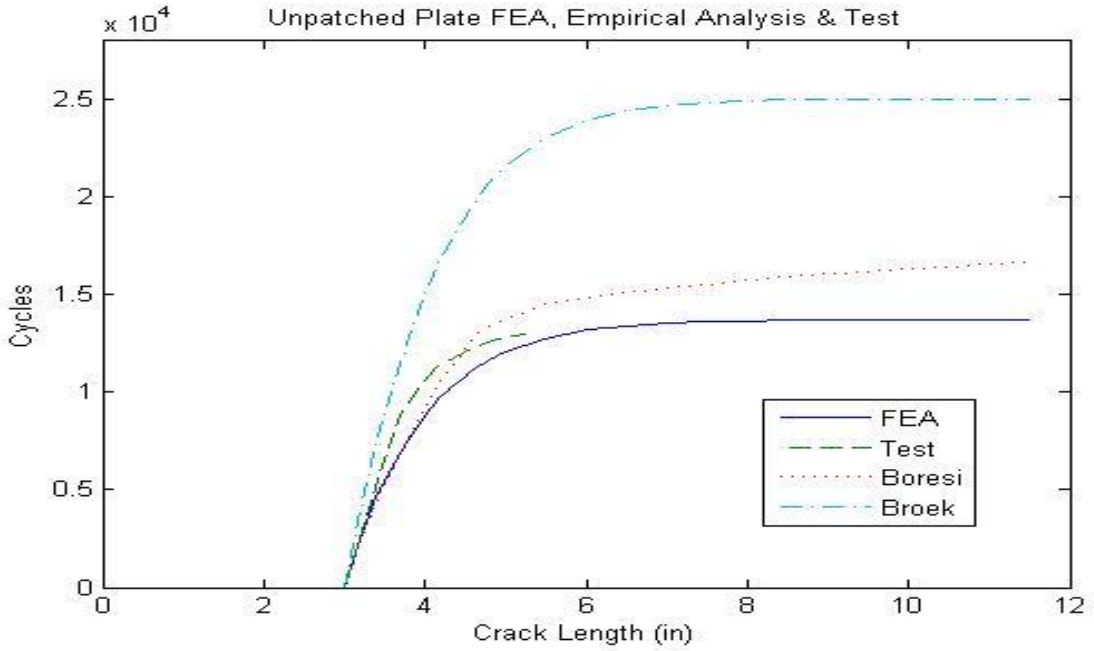


**Figure 6-17: FEA, Experimental and Empirical Analysis Results of Unpatched Plate**

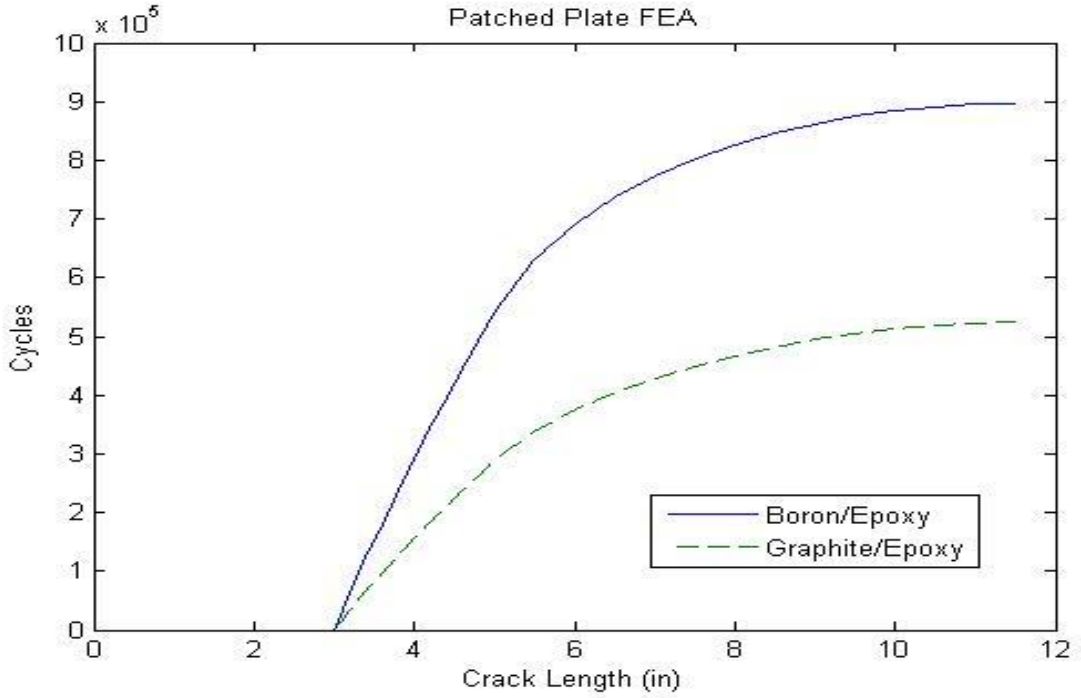

**Figure 6-18: FEA Results of Patched Plate**

## 6.5 Fatigue Test Results

As stated earlier in this report, tests were conducted on steel plates with and without the use of reinforcements. Recall that a cyclic tensional load oscillating between 2.0 and 50.0 kips was applied at one end of the plates. The first tests were on unpatched plates. No displacement data were collected for unpatched plate 1. Data for markers relative displacements versus cycles were collected on plates 2 and 3 and then plotted for the various test configurations. Shown in Figures 6-19 and 6-20 are the cycle histories for several marker locations for testing of the unpatched plate no. 2. The relative displacement between the markers increased more rapidly for those markers located directly above the initial crack than those located further away from the crack.

Both plates 2 and 3 had an initial 3.0 inch crack at mid span. Results are presented in Figure 6-21. In both cases, the number of cycles before the specimens failed was between 12,000 and 14,000. A crack length of at least 5.0 inches was reached in both plates before fracture of the members occurred. Once the crack became approximately 5.25 inches in length the plates failed abruptly.

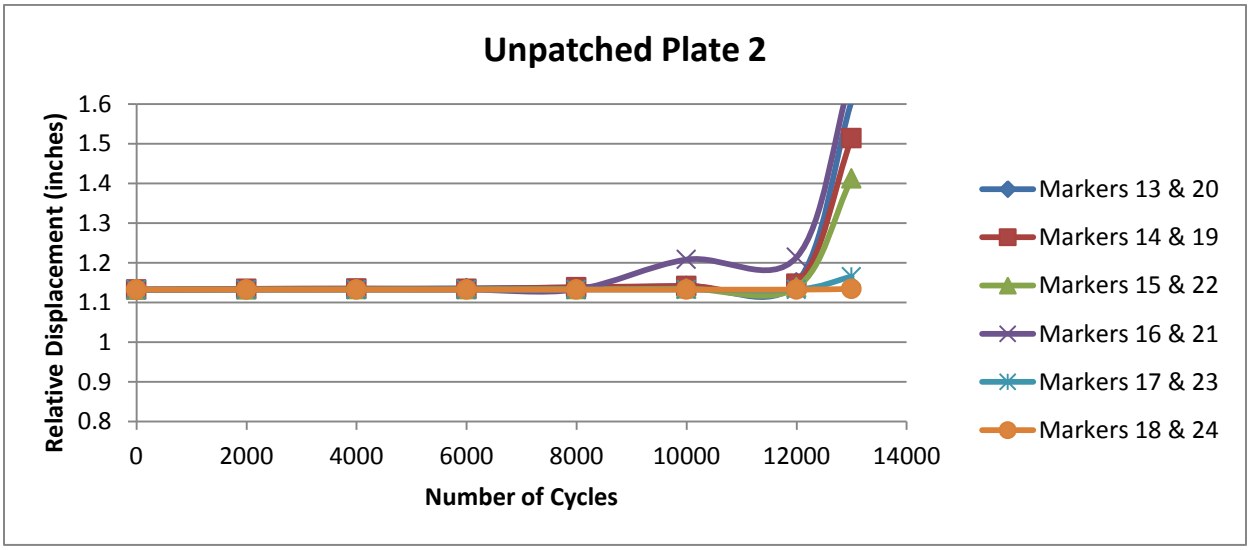


**Figure 6-19.** Marker's relative displacements for the unpatched configuration

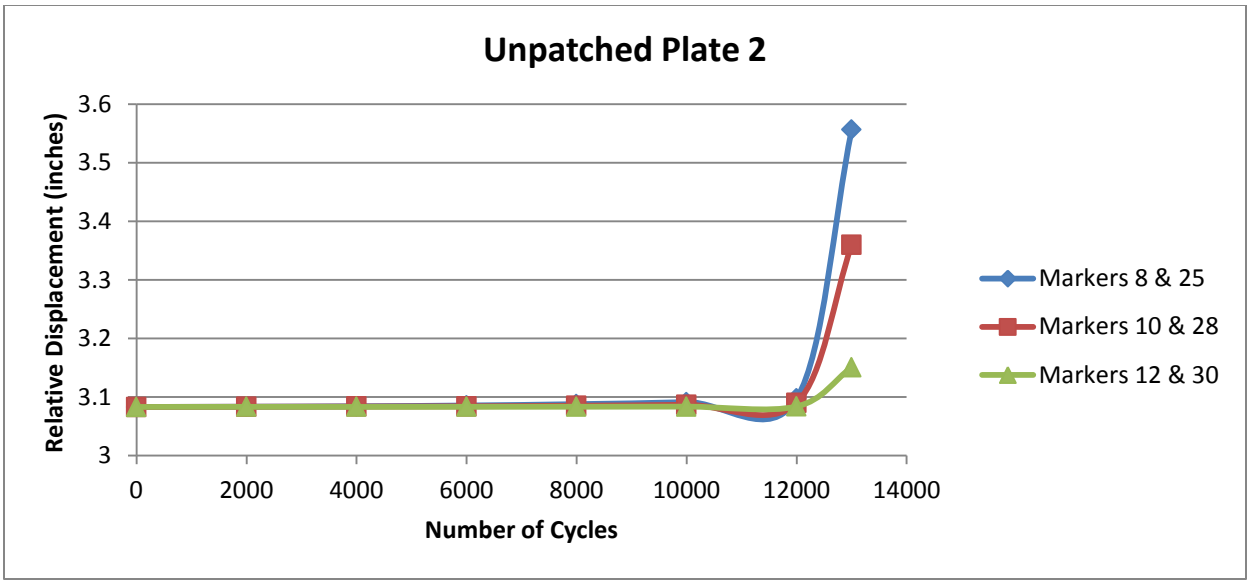


**Figure 6-20**. Marker's relative displacements for the unpatched configuration

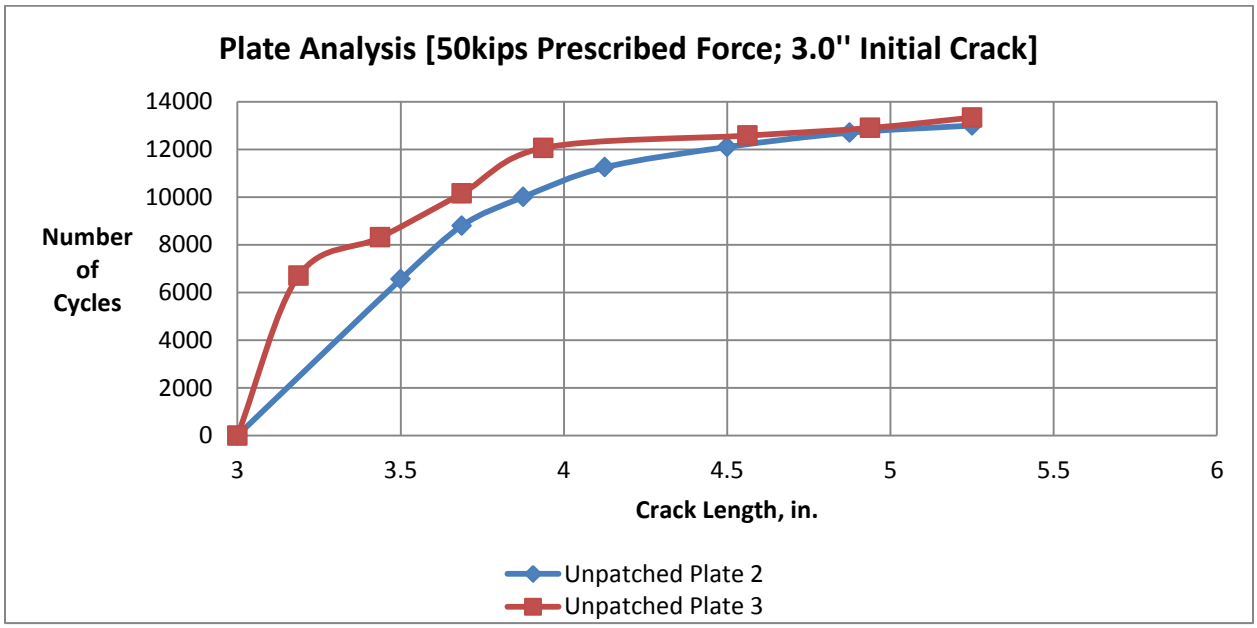


**Figure 6-21.** Crack growth data for plates without reinforcements

As in the previous tests, Optotrak data was utilized to determine the displacement field as a function of the cyclic tensile load for the patchedplates. Under normal conditions, the distance between markers placed closer to the initial crack should increase more rapidly with an increase in the number of cycles than those positioned further away from the crack. Findings are presented in the Figures 6-22, 23, and 24 below.

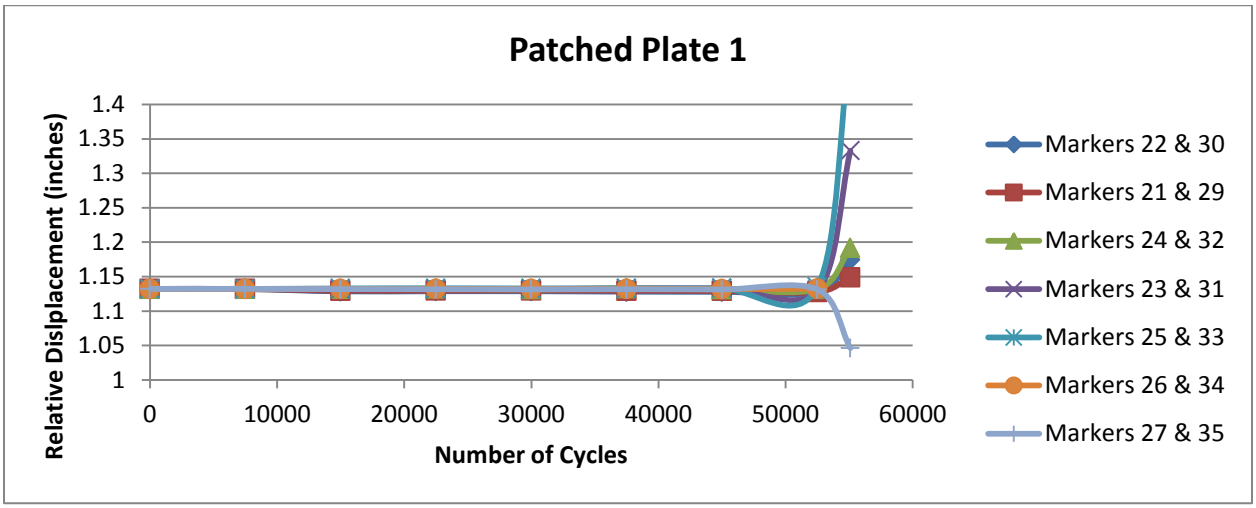


**Figure 6-22** Markers displacements for the reinforced configuration

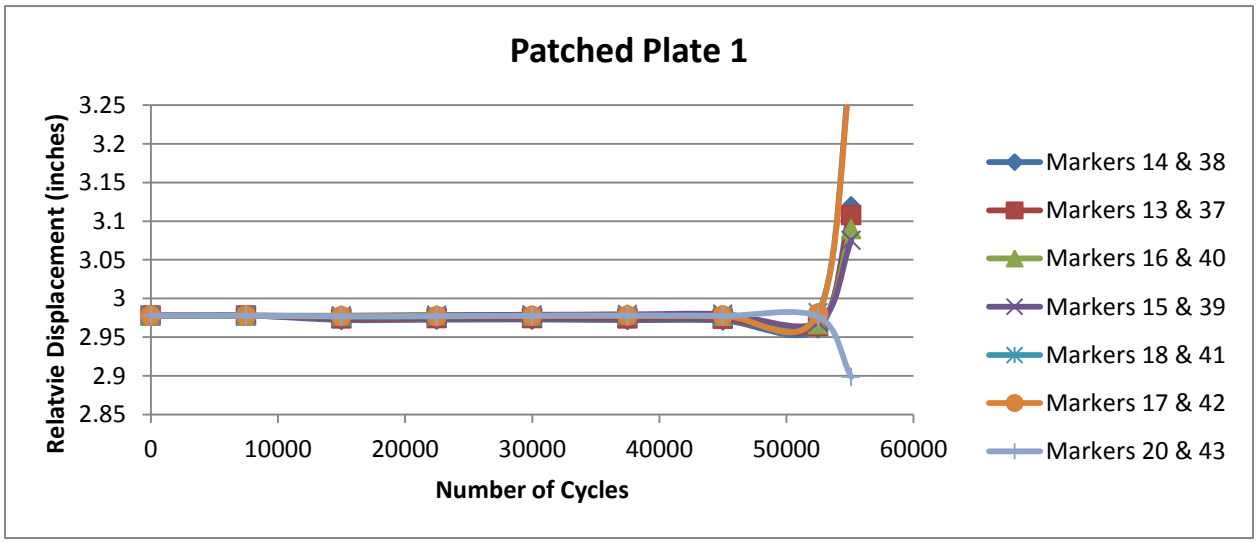


**Figure 6-23.** Markers displacements for the reinforced configuration

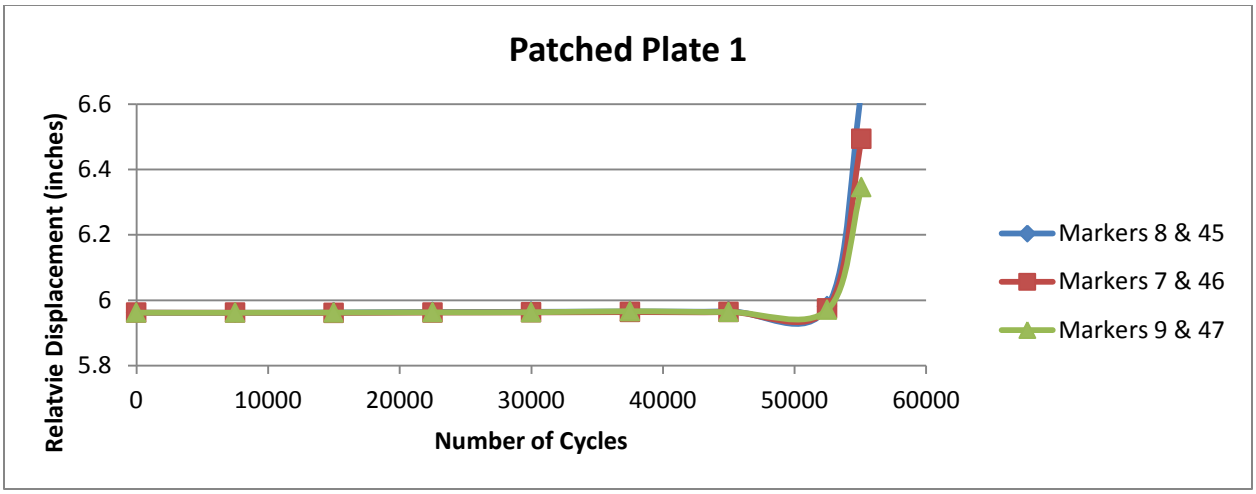


**Figure 6-24.** Markers displacements for the reinforced configuration

By observing the relative distance between two markers located on the same side of the crack (either above or below it), and if one sensor is located directly on the patch while the other sensor is placed directly on the plate, one can determine whether the patch was properly attached to the plate, or if sliding between the patch and the plate occurred. If the patch and the plate were efficiently attached, both members would move vertically the same amount as cyclic load is applied. Then, we should expect the distance between the two markers to be constant. On the other hand, if the patch is not perfectly attached to the plate, the relative distance between these markers should not be constant.

As Figure 6-25 shows, the relative distance between markers 8 and 14 is approximately constant for the first 50,000 cycles of testing. At cycle number 50,307, as recorded in the experiment, debonding between the patch and the plate occurred. Also, visible cracks in the patch itself were found at this number of cycles. Due to this debonding and patch cracking, the distance between the two markers suffered a slight increase, since the marker located on the patch moved slightly down along with the patch. Just before rupture of the specimen, this relative distance increased even more. Figures 6-22 through 6-25 show how that data obtained with the OptoTRAK camera system is consistent with what was perceived during the experiment.

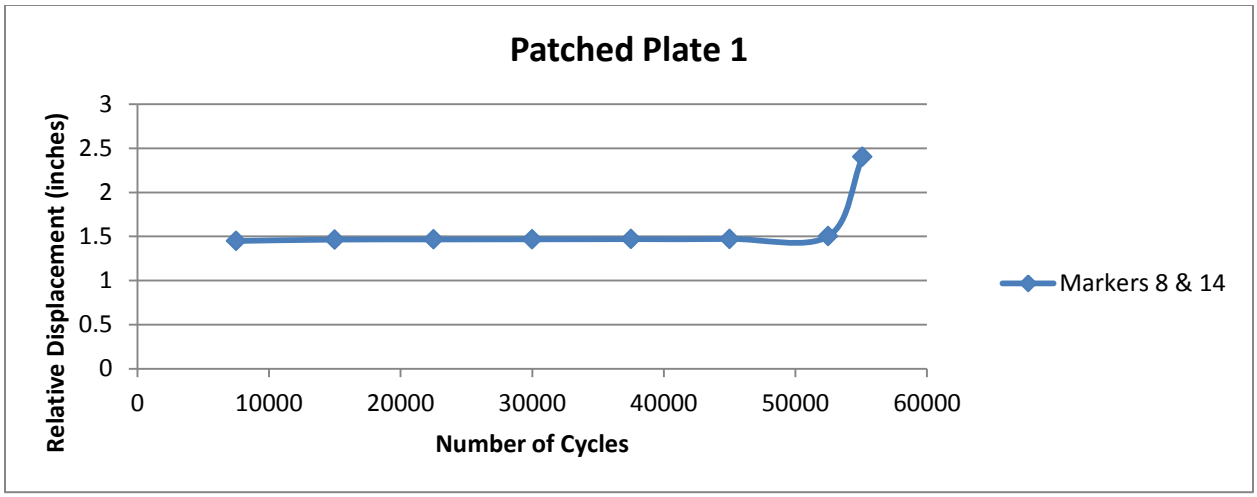


**Figure 6-25.** Relative Displacements Used to Determine Sliding of the Patch.

Crack length as a function of the total number of cycles was also determined for the reinforced plates. Two plates were studied using the high-strength flexible patch, and two specimens were tested, using a high-strength rigid patch attached. Having the composite patches attached on both sides of the plates prevented the research team from collecting crack growth data until fractures appeared in the patch. Therefore, measurements began to be taken immediately after the crack became visible on both the plate and patch. Results are presented below in Figure 26.

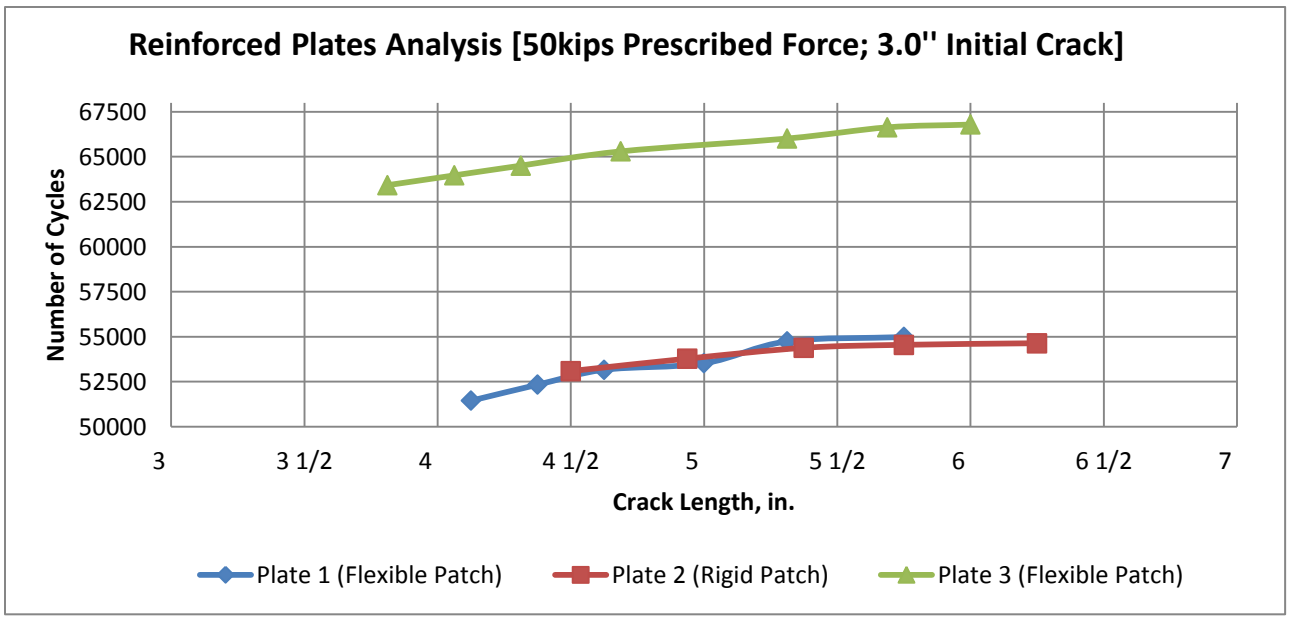


**Figure 6-26.** Crack growth data for plates with reinforcements.

As Figure 6-26 above shows, with the use of reinforcements, plate fracture due to fatigue did not occur until at least 54,000 cycles were reached for the first two plates, while approximately 66,000 cycles were required for rupture of the third specimen. These results show how the use of reinforcements has increased the fatigue life of the plates by approximately 400%. This is a clear indication that the use of composite patches effectively increases the fatigue life of structural members.

Not shown in these figures are the results of our fourth patched plate with a rigid patch. This test reached over 140,000 cycles with no indication of patch sliding, debonding or cracking of the patch itself. This is now approaching at least the order of magnitude of predicted fatigue life from the finite element predictions of section 6.4. Unfortunately we do not have final results for failure of this test. The test machine itself suffered fatigue damage of the connection bolts. This occurred even though the tests were being operated within the listed capacity of the test machine. On the plus side of this situation though is the fact that the composite patch system outlasted the testing machine, a positive outcome in itself.

# 7. Conclusions

Two configurations were investigated. Steel plates having a length of 18.0 in, a width of 12.0 in, and a thickness of 0.25 in, with a 3.0 inches initial crack at mid span were first studied without the use of reinforcements. Other plates of similar geometry were then examined using double-sided reinforcements. A cyclic load oscillating between 2.0 and 50.0 kips was applied at one end of the plates. Prior to these tests, simple tensile strength tests were conducted to establish the material properties of the composite patches and the steel panels.

Tests were conducted on the steel plates to experimentally validate the effectiveness of using composite patches as a means to prevent crack growth and extend the fatigue life of structural components. Specimens were tested with and without the use of reinforcements in order to corroborate finite element analyses. It is concluded that the finite element method can be used very effectively with accurate predictions of crack growth particularly for the unpatched plates. Finite element analyses, test results and analytical formulations ( e.g. using the correction factors of Boresi et al.) agree remarkably well.

Numerical simulations of the cracked plates indicate roughly two orders of magnitude increase in service life for the conditions tested although test results show increases closer to a single order of magnitude increase. This difference is attributed to two factors: debonding of the patch and actual cracking of the patch. Neither of these failure modes was taken into account in the finite element analyses. The debonding of the patch can also be improved by careful attention to the quality of the bonding process. We were actually learning by doing in this case and found that the thickness and uniformity of the layer of the epoxy is critical. It was also learned that application of normal pressure to the bond surface after attachment also improves the effectiveness of the patching. The effectiveness composite patching of steel plates have be demonstrated in this project. Considerable improvements in results are believed to be achievable; of critical importance are two factors: implementation of a quality-controlled bonding procedure and optimization of the geometry and properties of the patch systems dependent upon the parent plate’s properties and fracture conditions.

# 8. References


Allan R.C, Bird J, Clarke J.D. Overview-Use of adhesives in repair of cracks in ship structures. *Materials Science and Technology* October 1988; 4:853-859.

Allan, R. C., J. Bird, and J. D. Clarke. "Use of adhesives in repair of cracks in ship structures." *Materials Science and Technology* 4.10 1988: 853-859.

Belason, E., "Bonded doublers for aircraft structure repair," *Aerospace Engineering*, 1995: 17-26.

Bone J.S. Testing of Composite Patches for ship plating fracture repair. In: Naval Architecture and Marine Engineering. Master's Thesis, Ann Arbor, USA: University of Michigan. 2002.

Bocciarelli, Massimiliano, et al. "Fatigue performance of tensile steel members strengthened with CFRP plates." *Composite Structures* 87.4 2009: 334-343.

Boresi, A.P., Schmidt, R.J., Sidebottom, O.M., Advanced Mechanics of Materials, Fifth Edition, John Wiley & Sons, Inc., New York, 1993.

Buyukozturk, Oral, Oguz Gunes, and Erdem Karaca. "Progress on understanding debonding problems in reinforced concrete and steel members strengthened using FRP composites." *Construction and Building Materials* 18.1 2004: 9-19.

Colombi, Pierluigi, Andrea Bassetti, and Alain Nussbaumer. "Analysis of cracked steel members reinforced by pre-stress composite patch." *Fatigue & Fracture of Engineering Materials & Structures* 26.1 2003: 59-66.

Colombi, Pierluigi, Andrea Bassetti, and Alain Nussbaumer. "Delamination effects on cracked steel members reinforced by prestressed composite patch." *Theoretical and Applied Fracture Mechanics* 39.1 2003: 61-71.

Edwards, Matthew "Analysis of Composite Patches for Ship Plating Fracture Repair" In: Naval Architecture and Marine Engineering. Master's Thesis, Ann Arbor, USA: University of Michigan. 1999.

Edwards, M. and Karr, D.G., ”Analysis of composite patches for ship plating fracture repair”, *Ship Technology Research*, Vol. 46, 1999: pp. 231-238.

Grabovac I, Bartholomeusz R.A, Baker A.A. Composite reinforcement of a ship superstructure-project overview. *Composites* 1993: 24:501-509.

Grabovac I, Whittaker D. Application of bonded composites in repair of ships structures – A 15-year service experience. *Composites: Part A* 2009: 40:1381-1389.

Grabovac I. Bonded composite solution to ship reinforcement. *Composites: Part A* 2003; 34:847-854.

Harris, E., and Z. Olshenske. "Aligned discontinuous fiber-based formable textiles for aircraft composite repair." *SAMPE Journal* 46, no. 3 2010: 16-25.

Hosseini-Toudeshky H, Mohammedi B, Sadeghi G, Daghyani H.R. Numerical and experimental fatigue crack growth analysis in mode-I for repaired aluminum panels using composite material. *Composites: Part A* 2007; 38:1141-1148.

Huawen, Ye, et al. "Fatigue performance of tension steel plates strengthened with prestressed CFRP laminates." *Journal of Composites for Construction* 14.5 2010: 609-615.

Jones, Sean C., and Scott A. Civjan. "Application of fiber reinforced polymer overlays to extend steel fatigue life." *Journal of Composites for Construction* 7.4 2003: 331-338.

Khalili S.M.R, Ghadjar R, Sadeghinia M ,Mittal R.K. An experimental study on the Charpy impact response of cracked aluminum plates repaired with GFRP or CFRP composite patches. *Composite Structures* 2009; 89:270-274.

Khalili, S. M. R., M. Shiravi, and A. S. Nooramin. "Mechanical behavior of notched plate repaired with polymer composite and smart patches-experimental study." *Journal of Reinforced Plastics and Composites* 29.19 2010: 3021-3037.

Lam, Angus CC, et al. "Repair of steel structures by bonded carbon fibre reinforced polymer patching: experimental and numerical study of carbon fibre reinforced polymer-steel double-lap joints under tensile loading." *Canadian Journal of Civil Engineering* 34.12 2007: 1542-1553.

Lam, Angus CC, et al. "Study of stress intensity factor of a cracked steel plate with a single-side cfrp composite patching." *Journal of Composites for Construction* 14.6 2010: 791-803.

Lena, M.R., Klug, J.C., Sun, C.T., “Composite patches as reinforcements and crack arrestors in aircraft structures,” *Journal of Aircraft*, Vol. 35, No. 2, Mar-Apr 1998: 318-323.

Liu, Hongbo, et al. "Prediction of fatigue life for CFRP-strengthened steel plates." *Thin-Walled Structures* 47.10 2009: 1069-1077.

Liu, Hongbo, Riadh Al-Mahaidi, and Xiao-Ling Zhao. "Experimental study of fatigue crack growth behaviour in adhesively reinforced steel structures." *Composite Structures* 90.1 2009: 12-20.

Okafor, A. Chukwujekwu, Navdeep Singh, U. E. Enemuoh, and S. V. Rao. "Design, analysis and performance of adhesively bonded composite patch repair of cracked aluminum aircraft panels." *Composite Structures* 71, no. 2 2005: 258-270.

Righiniotis, T. D., E. S. Aggelopoulos, and M. K. Chryssanthopoulos. "Fracture mechanics 2D-FEA of a cracked steel plate with a CFRP patch." Hollaway L C. *Advanced Polymer Composites for Structural Applications in Construction*: ACIC 2004: 284-291.

Roy, M., C. Lang, and I. M. May. "Modelling composite repairs to cracked metal structures." *Proceedings of the Institution of Civil Engineers. Structures and Buildings* 162.2 2009: 107-113.

Rybicki, E.F., Kanninen, M.F., “A finite element calculation of stress intensity factors by a modified crack closure integral,” *Engineering Fracture Mechanics*, Vol. 9, 1977: 931-938.

Seo Dae-Cheol, Lee Jung-Ju. Fatigue crack growth behavior of cracked aluminum plate repaired with composite patch. *Composite Structures* 2002; 57:323-330.

Shenoi, R.M. et al. “Composite Materials for Marine Applications: Key Challenges for the Future” in Nicolais, Luigi, Michele Meo, and Eva Milella, eds. Composite Materials: A Vision for the Future. Springer, 2011.

Tavakkolizadeh, Mohammadreza, and H. Saadatmanesh. "Fatigue strength of steel girders strengthened with carbon fiber reinforced polymer patch." *Journal of Structural Engineering* 129.2 2003: 186-196.

Tsouvalis, Nicholas G., Lazarus S. Mirisiotis, and Dimitris N. Dimou. "Experimental and numerical study of the fatigue behaviour of composite patch reinforced cracked steel plates." *International Journal of Fatigue* 31.10 2009: 1613-1627.

Turton T.J, Dalzel-Job J, Livingstone F. Oil platforms, destroyers and frigates-case studies of QinetiQ's marine composite patch repairs. *Composites: Part A* 2005; 36:1066-1072.

Wang Q.Y, Pidaparti R.M. Static characteristics and fatigue behavior of composite-repaired aluminum plates. *Composite Structures* 2002; 56:151-155.

Wang Q.Y, Sriraman M.R, Kawagoishi N, Chen Q. Fatigue crack growth of bonded composite repairs in gigacycle regime. *International Journal of Fatigue* 2006; 28:1197-1201.

Wiernicki, C.J., "Residual Strength in Damage Marine Structures," *Ship Structure Committee Report No. 381*, 1995.

Xiong J.J, Shenoi R.A. Integrated experimental screening of bonded composites patch repair schemes to notched aluminum-alloy panels based on static and fatigue strength concepts. *Composite Structures* 2008; 83:266-272.

Zhao, Xiao-Ling, and Lei Zhang. "State-of-the-art review on FRP strengthened steel structures." *Engineering Structures* 29.8 2007: 1808-1823.

# 9.0 Acknowledgements

This report was made possible by the contributions of several co-authors of the report:

Tony J. Cao performed a plate usage study contacting U.S. Coast Guard, U.S. Navy and American Bureau of Shipping (ABS) individuals. Caner Baloglu performed a composite patch usage study which summarizes recent studies available in the literature with an emphasis on ship plating repair. Kok Tong Ong performed finite element analyses of metal plates with edge cracks without reinforcement and with composite patch reinforcements. Andre Douglas and Bo Rohrback performed finite element analyses of metal plates with double edge cracks without reinforcement and with composite patch reinforcements. Kurt Nielsen and Nan Si performed the finite element analyses of the test configurations. Carlos Ferrarri, Kurt Neilsen, Nan Si, Paul White, and Professor Gustavo J. Parra-Montesinos were instrumental in planning, performing, and data acquisition for the fatigue tests.

# Appendix A: Example Photographs of Cracked Plating


# Appendix B - Sample Calculations

The following data for the sample calculation is from Dataset #3 Boron/Epoxy Patch, plate thickness 0.5”, crack length 2”. The highlighted cells are data extracted from the relevant FEA model.

| | Crack Tip (b) | | | Adjacent Node (a) | | | | | Discretized | |
|---|---|---|---|---|---|---|---|---|---|---|
| a (in) | $F_y^b$ (klbs) | | Total (lb) | $u_y^a$ (in) | | Ave | Energy Release Rate G | Experimental K (lbs/in^1.5) | ΔN | N |
| 0.5 | -0.2411 | -0.2431 | 484.253 | 1.5105E-04 | 2.7895E-04 | 2.1500E-04 | 5.2057 | 24994 | 8.43E+03 | 8.43E+03 |
| 1 | -0.2763 | -0.2787 | 555.077 | 1.7259E-04 | 3.2218E-04 | 2.4739E-04 | 6.8659 | 28704 | 5.56E+03 | 1.40E+04 |
| 1.5 | -0.2910 | -0.2935 | 584.523 | 1.8165E-04 | 3.3981E-04 | 2.6073E-04 | 7.6201 | 30239 | 4.76E+03 | 1.88E+04 |
| 2 | -0.2992 | -0.3018 | 601.056 | 1.8675E-04 | 3.4961E-04 | 2.6818E-04 | 8.0595 | 31099 | 4.38E+03 | 2.31E+04 |

The FEA model is a 3D model with 2 nodes at each crack length. Hence, there are two values for the force at the crack tip and displacement of the adjacent node in the y-direction. The total crack tip force is summation of absolute forces at the crack tip. Note the difference in units. The displacement at the adjacent node is the average y-displacement of both nodes.

Energy Release Rate $G_u$ $= \dfrac{F_y^b u_a^y}{\Delta a}$

$= \dfrac{601.056 \times 2.6818 \times 10^{-4}}{0.02}$

$= 8.0595$ lb

Stress Intensity Factor K $= \sqrt{\dfrac{G_u E_s}{t_s}}$

$= \sqrt{\dfrac{8.0595 \times 30 \times 10^6}{0.25}}$

$= 31099$ lbs/in$^{1.5}$

$$= 31099\frac{4.4482216}{25.4^{1.5}}$$

$= 1081\ \text{N/mm}^{1.5}$

$$\Delta N_2 = \frac{a_j - a_{j-1}}{CK^m}$$

$$= \frac{25.4(2-1.5)}{2.3\times10^{-12}\times1081^3}$$

$= 4.38\text{x}10^3$ cycles

$$N = \sum_{a=0}^{2}\Delta N_a$$

$= (8.43+5.56+4.76+4.38)\text{x}10^3$

$= 2.31\text{x}10^4$ cycles

# Appendix C - Datasets

1. Comparing Geometry Correction Factor

| | | |
|---|---|---|
| Load σ | 30000 | psi |
| Steel Young's Modulus | 30000000 | psi |
| Plate Length | 36 | in |

| | | Brock | | Wirenicki | | Boresi | | | | | |
|---|---|---|---|---|---|---|---|---|---|---|---|
| a (in) | K1 (w/o correction) | Y | K1 | Y | K1 | λ | λ' | f1(λ) | f2(λ) | f(λ) | K1 |
| 0.5 | 37599 | 1.0222 | 38435 | 1.0005 | 37617 | 0.0556 | 0.1 | 1.01 | 1.01 | 1.0100 | 37975 |
| 1 | 53174 | 1.0453 | 55581 | 1.0019 | 53275 | 0.1111 | 0.1 | 1.03 | 1.01 | 1.0122 | 53824 |
| 1.5 | 65124 | 1.0692 | 69632 | 1.0043 | 65404 | 0.1667 | 0.1 | 1.03 | 1.01 | 1.0233 | 66644 |
| 2 | 75199 | 1.0941 | 82275 | 1.0077 | 75777 | 0.2222 | 0.2 | 1.06 | 1.03 | 1.0367 | 77956 |
| 2.5 | 84075 | 1.1200 | 94161 | 1.0121 | 85089 | 0.2778 | 0.2 | 1.06 | 1.03 | 1.0533 | 88559 |
| 3 | 92099 | 1.1469 | 105627 | 1.0175 | 93710 | 0.3333 | 0.3 | 1.11 | 1.06 | 1.0767 | 99160 |
| 3.5 | 99479 | 1.1749 | 116878 | 1.0240 | 101864 | 0.3889 | 0.3 | 1.11 | 1.06 | 1.1044 | 109869 |
| 4 | 106347 | 1.2041 | 128054 | 1.0316 | 109707 | 0.4444 | 0.4 | 1.19 | 1.11 | 1.1456 | 121827 |
| 4.5 | 112798 | 1.2346 | 139258 | 1.0404 | 117353 | 0.5000 | 0.5 | 1.19 | 1.19 | 1.1900 | 134230 |
| 5 | 118900 | 1.2664 | 150572 | 1.0504 | 124895 | 0.5556 | 0.5 | 1.3 | 1.19 | 1.2511 | 148757 |
| 5.5 | 124703 | 1.2996 | 162065 | 1.0618 | 132408 | 0.6111 | 0.6 | 1.3 | 1.3 | 1.3241 | 165116 |
| 6 | 130248 | 1.3344 | 173797 | 1.0746 | 139961 | 0.6667 | 0.6 | 1.3 | 1.3 | 1.4444 | 188136 |
| 8 | 150398 | 1.4908 | 224215 | 1.1425 | 171836 | 0.8889 | 0.6 | 1.3 | 1.3 | 1.9259 | 289655 |
| 10 | 168150 | 1.6821 | 282847 | 1.2473 | 209731 | 1.1111 | 0.6 | 1.3 | 1.3 | 2.4074 | 404805 |

2. No Patch, Plate Thickness 0.5”

| | Crack Tip (b) | | | Adjacent Node (a) | | | | | Discretized | |
|---|---|---|---|---|---|---|---|---|---|---|
| a (in) | $F_y^b$ (klbs) | | Total (lb) | $u_y^a$ (in) | | Ave | Energy Release Rate G | Experimental K (lbs/in^1.5) | ΔN | N |
| 0.5 | -0.3597 | -0.3610 | 720.665 | 3.2090E-04 | 3.3221E-04 | 3.2655E-04 | 11.7668 | 37577 | 2.48E+03 | 2.48E+03 |
| 1 | -0.5087 | -0.5108 | 1019.528 | 4.5178E-04 | 4.7902E-04 | 4.6540E-04 | 23.7246 | 53357 | 8.66E+02 | 3.35E+03 |
| 1.5 | -0.6257 | -0.6284 | 1254.113 | 5.5497E-04 | 5.9287E-04 | 5.7392E-04 | 35.9882 | 65716 | 4.64E+02 | 3.81E+03 |
| 2 | -0.7275 | -0.7307 | 1458.178 | 6.4486E-04 | 6.9143E-04 | 6.6815E-04 | 48.7138 | 76457 | 2.94E+02 | 4.10E+03 |
| 2.5 | -0.8208 | -0.8244 | 1645.236 | 7.2731E-04 | 7.8154E-04 | 7.5443E-04 | 62.0604 | 86297 | 2.05E+02 | 4.31E+03 |
| 3 | -0.9092 | -0.9132 | 1822.482 | 8.0546E-04 | 8.6679E-04 | 8.3612E-04 | 76.1911 | 95619 | 1.51E+02 | 4.46E+03 |
| 3.5 | -0.9950 | -0.9994 | 1994.37 | 8.8127E-04 | 9.4936E-04 | 9.1532E-04 | 91.2741 | 104656 | 1.15E+02 | 4.57E+03 |
| 4 | -1.0796 | -1.0844 | 2163.93 | 9.5607E-04 | 1.0308E-03 | 9.9342E-04 | 107.4840 | 113570 | 8.98E+01 | 4.66E+03 |
| 4.5 | -1.1641 | -1.1693 | 2333.35 | 1.0308E-03 | 1.1120E-03 | 1.0714E-03 | 125.0011 | 122475 | 7.16E+01 | 4.74E+03 |
| 5 | -1.2494 | -1.2549 | 2504.32 | 1.1063E-03 | 1.1940E-03 | 1.1501E-03 | 144.0159 | 131461 | 5.79E+01 | 4.79E+03 |
| 5.5 | -1.3361 | -1.3420 | 2678.14 | 1.1830E-03 | 1.2774E-03 | 1.2302E-03 | 164.7270 | 140596 | 4.74E+01 | 4.84E+03 |
| 6 | -1.4248 | -1.4311 | 2855.89 | 1.2614E-03 | 1.3626E-03 | 1.3120E-03 | 187.3450 | 149938 | 3.90E+01 | 4.88E+03 |
| 8 | -1.8075 | -1.8156 | 3623.04 | 1.5999E-03 | 1.7303E-03 | 1.6651E-03 | 301.6326 | 190252 | 7.64E+01 | 4.96E+03 |
| 10 | -2.2536 | -2.2637 | 4517.3 | 1.9945E-03 | 2.1590E-03 | 2.0767E-03 | 469.0640 | 237250 | 3.94E+01 | 5.00E+03 |

3. Boron/Epoxy Patch, Plate Thickness 0.5”

| | Crack Tip (b) | | | Adjacent Node (a) | | | | | Discretized | |
|---|---|---|---|---|---|---|---|---|---|---|
| a (in) | $F_y^b$ (klbs) | | Total (lb) | $u_y^a$ (in) | | Ave | Energy Release Rate G | Experimental K (lbs/in^1.5) | ΔN | N |
| 0.5 | -0.2411 | -0.2431 | 484.253 | 1.5105E-04 | 2.7895E-04 | 2.1500E-04 | 5.2057 | 24994 | 8.43E+03 | 8.43E+03 |
| 1 | -0.2763 | -0.2787 | 555.077 | 1.7259E-04 | 3.2218E-04 | 2.4739E-04 | 6.8659 | 28704 | 5.56E+03 | 1.40E+04 |
| 1.5 | -0.2910 | -0.2935 | 584.523 | 1.8165E-04 | 3.3981E-04 | 2.6073E-04 | 7.6201 | 30239 | 4.76E+03 | 1.88E+04 |
| 2 | -0.2992 | -0.3018 | 601.056 | 1.8675E-04 | 3.4961E-04 | 2.6818E-04 | 8.0595 | 31099 | 4.38E+03 | 2.31E+04 |
| 2.5 | -0.3048 | -0.3074 | 612.239 | 1.9021E-04 | 3.5619E-04 | 2.7320E-04 | 8.3632 | 31679 | 4.14E+03 | 2.73E+04 |
| 3 | -0.3091 | -0.3118 | 620.864 | 1.9289E-04 | 3.6124E-04 | 2.7707E-04 | 8.6010 | 32127 | 3.97E+03 | 3.12E+04 |
| 3.5 | -0.3127 | -0.3155 | 628.198 | 1.9516E-04 | 3.6553E-04 | 2.8034E-04 | 8.8056 | 32506 | 3.83E+03 | 3.51E+04 |
| 4 | -0.3161 | -0.3188 | 634.917 | 1.9725E-04 | 3.6944E-04 | 2.8334E-04 | 8.9950 | 32854 | 3.71E+03 | 3.88E+04 |
| 4.5 | -0.3193 | -0.3221 | 641.459 | 1.9928E-04 | 3.7324E-04 | 2.8626E-04 | 9.1813 | 33193 | 3.60E+03 | 4.24E+04 |
| 5 | -0.3227 | -0.3255 | 648.274 | 2.0140E-04 | 3.7720E-04 | 2.8930E-04 | 9.3773 | 33545 | 3.49E+03 | 4.59E+04 |
| 5.5 | -0.3268 | -0.3297 | 656.53 | 2.0397E-04 | 3.8197E-04 | 2.9297E-04 | 9.6173 | 33972 | 3.36E+03 | 4.92E+04 |
| 6 | -0.3398 | -0.3430 | 682.775 | 2.0908E-04 | 4.0017E-04 | 3.0463E-04 | 10.3996 | 35326 | 2.99E+03 | 5.22E+04 |
| 8 | -0.6029 | -0.6054 | 1208.316 | 5.3486E-04 | 5.7049E-04 | 5.5267E-04 | 33.3902 | 63299 | 2.08E+03 | 5.43E+04 |
| 10 | -0.8064 | -0.8099 | 1616.328 | 7.1460E-04 | 7.6746E-04 | 7.4103E-04 | 59.8874 | 84773 | 8.64E+02 | 5.51E+04 |

4. Graphite/Epoxy Patch, Plate Thickness 0.5”

| | Crack Tip (b) | | | Adjacent Node (a) | | | | | Discretized | |
|---|---|---|---|---|---|---|---|---|---|---|
| a (in) | $F_y^b$ (klbs) | | Total (lb) | $u_y^a$ (in) | | Ave | Energy Release Rate G | Experimental K (lbs/in^1.5) | ΔN | N |
| 0.5 | -0.2587 | -0.2609 | 519.631 | 1.6402E-04 | 2.9813E-04 | 2.3107E-04 | 6.0036 | 26841 | 6.81E+03 | 6.81E+03 |
| 1 | -0.3018 | -0.3044 | 606.222 | 1.9067E-04 | 3.5076E-04 | 2.7072E-04 | 8.2058 | 31380 | 4.26E+03 | 1.11E+04 |
| 1.5 | -0.3205 | -0.3233 | 643.785 | 2.0236E-04 | 3.7319E-04 | 2.8777E-04 | 9.2632 | 33340 | 3.55E+03 | 1.46E+04 |
| 2 | -0.3311 | -0.3339 | 664.989 | 2.0898E-04 | 3.8574E-04 | 2.9736E-04 | 9.8869 | 34445 | 3.22E+03 | 1.78E+04 |
| 2.5 | -0.3381 | -0.3410 | 679.066 | 2.1338E-04 | 3.9402E-04 | 3.0370E-04 | 10.3115 | 35176 | 3.02E+03 | 2.09E+04 |
| 3 | -0.3433 | -0.3463 | 689.545 | 2.1666E-04 | 4.0015E-04 | 3.0841E-04 | 10.6331 | 35721 | 2.89E+03 | 2.37E+04 |
| 3.5 | -0.3475 | -0.3505 | 698.05 | 2.1933E-04 | 4.0512E-04 | 3.1222E-04 | 10.8974 | 36162 | 2.78E+03 | 2.65E+04 |
| 4 | -0.3512 | -0.3542 | 705.446 | 2.2165E-04 | 4.0943E-04 | 3.1554E-04 | 11.1298 | 36546 | 2.70E+03 | 2.92E+04 |
| 4.5 | -0.3546 | -0.3577 | 712.277 | 2.2380E-04 | 4.1340E-04 | 3.1860E-04 | 11.3464 | 36900 | 2.62E+03 | 3.18E+04 |
| 5 | -0.3580 | -0.3611 | 719.036 | 2.2592E-04 | 4.1732E-04 | 3.2162E-04 | 11.5628 | 37250 | 2.55E+03 | 3.44E+04 |
| 5.5 | -0.3619 | -0.3650 | 726.879 | 2.2839E-04 | 4.2185E-04 | 3.2512E-04 | 11.8161 | 37655 | 2.46E+03 | 3.69E+04 |
| 6 | -0.3759 | -0.3794 | 755.259 | 2.3464E-04 | 4.4049E-04 | 3.3757E-04 | 12.7475 | 39111 | 2.20E+03 | 3.91E+04 |
| 8 | -0.6370 | -0.6397 | 1276.698 | 5.6503E-04 | 6.0328E-04 | 5.8416E-04 | 37.2896 | 66894 | 1.76E+03 | 4.08E+04 |
| 10 | -0.8396 | -0.8433 | 1682.933 | 7.4398E-04 | 7.9941E-04 | 7.7170E-04 | 64.9358 | 88274 | 7.65E+02 | 4.16E+04 |

5. No Patch, Plate Thickness 0.75”

| | Crack Tip (b) | | | Adjacent Node (a) | | | | | Discretized | |
|---|---|---|---|---|---|---|---|---|---|---|
| a (in) | $F_y^b$ (klbs) | | Total (lb) | $u_y^a$ (in) | | Ave | Energy Release Rate G | Experimental K (lbs/in^1.5) | ΔN | N |
| 0.5 | -0.5409 | -0.5426 | 1083.438 | 3.1654E-04 | 3.3430E-04 | 3.2542E-04 | 17.6285 | 37554 | 2.48E+03 | 2.48E+03 |
| 1 | -0.7652 | -0.7680 | 1533.182 | 4.4220E-04 | 4.8565E-04 | 4.6392E-04 | 35.5638 | 53340 | 8.67E+02 | 3.35E+03 |
| 1.5 | -0.9413 | -0.9449 | 1886.135 | 5.4193E-04 | 6.0238E-04 | 5.7215E-04 | 53.9577 | 65701 | 4.64E+02 | 3.82E+03 |
| 2 | -1.0944 | -1.0987 | 2193.14 | 6.2899E-04 | 7.0324E-04 | 6.6612E-04 | 73.0442 | 76443 | 2.95E+02 | 4.11E+03 |
| 2.5 | -1.2348 | -1.2397 | 2474.55 | 7.0894E-04 | 7.9537E-04 | 7.5215E-04 | 93.0620 | 86284 | 2.05E+02 | 4.32E+03 |
| 3 | -1.3679 | -1.3733 | 2741.19 | 7.8477E-04 | 8.8247E-04 | 8.3362E-04 | 114.2557 | 95606 | 1.51E+02 | 4.47E+03 |
| 3.5 | -1.4969 | -1.5029 | 2999.77 | 8.5837E-04 | 9.6681E-04 | 9.1259E-04 | 136.8778 | 104643 | 1.15E+02 | 4.58E+03 |
| 4 | -1.6242 | -1.6307 | 3254.83 | 9.3100E-04 | 1.0499E-03 | 9.9046E-04 | 161.1889 | 113557 | 8.99E+01 | 4.67E+03 |
| 4.5 | -1.7513 | -1.7584 | 3509.68 | 1.0036E-03 | 1.1329E-03 | 1.0683E-03 | 187.4608 | 122462 | 7.17E+01 | 4.74E+03 |
| 5 | -1.8796 | -1.8872 | 3766.86 | 1.0769E-03 | 1.2166E-03 | 1.1467E-03 | 215.9795 | 131447 | 5.79E+01 | 4.80E+03 |
| 5.5 | -2.0101 | -2.0182 | 4028.33 | 1.1514E-03 | 1.3017E-03 | 1.2265E-03 | 247.0414 | 140582 | 4.74E+01 | 4.85E+03 |
| 6 | -2.1435 | -2.1522 | 4295.71 | 1.2276E-03 | 1.3886E-03 | 1.3081E-03 | 280.9631 | 149923 | 3.91E+01 | 4.89E+03 |
| 8 | -2.7193 | -2.7304 | 5449.64 | 1.5565E-03 | 1.7639E-03 | 1.6602E-03 | 452.3678 | 190235 | 7.65E+01 | 4.96E+03 |
| 10 | -3.3904 | -3.4044 | 6794.78 | 1.9399E-03 | 2.2014E-03 | 2.0706E-03 | 703.4721 | 237229 | 3.94E+01 | 5.00E+03 |

6. Boron/Epoxy Patch, Plate Thickness 0.75”

| | Crack Tip (b) | | | Adjacent Node (a) | | | | | Discretized | |
|---|---|---|---|---|---|---|---|---|---|---|
| a (in) | $F_y^b$ (klbs) | | Total (lb) | $u_y^a$ (in) | | Ave | Energy Release Rate G | Experimental K (lbs/in^1.5) | ΔN | N |
| 0.5 | -0.4112 | -0.4150 | 826.17 | 1.5907E-04 | 3.3029E-04 | 2.4468E-04 | 10.1073 | 28436 | 5.72E+03 | 5.72E+03 |
| 1 | -0.4959 | -0.5006 | 996.551 | 1.9002E-04 | 4.0317E-04 | 2.9660E-04 | 14.7787 | 34385 | 3.24E+03 | 8.96E+03 |
| 1.5 | -0.5364 | -0.5415 | 1077.909 | 2.0511E-04 | 4.3730E-04 | 3.2120E-04 | 17.3115 | 37214 | 2.55E+03 | 1.15E+04 |
| 2 | -0.5604 | -0.5657 | 1126.066 | 2.1411E-04 | 4.5731E-04 | 3.3571E-04 | 18.9017 | 38886 | 2.24E+03 | 1.38E+04 |
| 2.5 | -0.5766 | -0.5821 | 1158.675 | 2.2023E-04 | 4.7078E-04 | 3.4551E-04 | 20.0166 | 40017 | 2.05E+03 | 1.58E+04 |
| 3 | -0.5887 | -0.5943 | 1182.992 | 2.2482E-04 | 4.8078E-04 | 3.5280E-04 | 20.8679 | 40859 | 1.93E+03 | 1.77E+04 |
| 3.5 | -0.5984 | -0.6041 | 1202.524 | 2.2851E-04 | 4.8879E-04 | 3.5865E-04 | 21.5641 | 41535 | 1.84E+03 | 1.96E+04 |
| 4 | -0.6067 | -0.6125 | 1219.208 | 2.3166E-04 | 4.9561E-04 | 3.6364E-04 | 22.1674 | 42112 | 1.76E+03 | 2.13E+04 |
| 4.5 | -0.6142 | -0.6201 | 1234.276 | 2.3452E-04 | 5.0176E-04 | 3.6814E-04 | 22.7192 | 42633 | 1.70E+03 | 2.30E+04 |
| 5 | -0.6215 | -0.6274 | 1248.809 | 2.3728E-04 | 5.0767E-04 | 3.7248E-04 | 23.2575 | 43135 | 1.64E+03 | 2.47E+04 |
| 5.5 | -0.6294 | -0.6353 | 1264.699 | 2.4032E-04 | 5.1411E-04 | 3.7722E-04 | 23.8534 | 43684 | 1.58E+03 | 2.63E+04 |
| 6 | -0.6502 | -0.6570 | 1307.193 | 2.4161E-04 | 5.3816E-04 | 3.8989E-04 | 25.4829 | 45151 | 1.43E+03 | 2.77E+04 |
| 8 | -1.0196 | -1.0235 | 2043.02 | 5.8682E-04 | 6.5300E-04 | 6.1991E-04 | 63.3241 | 71175 | 1.46E+03 | 2.91E+04 |
| 10 | -1.3210 | -1.3262 | 2647.21 | 7.5824E-04 | 8.5130E-04 | 8.0477E-04 | 106.5196 | 92312 | 6.69E+02 | 2.98E+04 |

7. Graphite Epoxy Patch, Plate Thickness 0.75”

| | Crack Tip (b) | | | Adjacent Node (a) | | | | | Discretized | |
|---|---|---|---|---|---|---|---|---|---|---|
| a (in) | $F_y^b$ (klbs) | | Total (lb) | $u_y^a$ (in) | | Ave | Energy Release Rate G | Experimental K (lbs/in^1.5) | ΔN | N |
| 0.5 | -0.4327 | -0.4366 | 869.245 | 1.6948E-04 | 3.4597E-04 | 2.5772E-04 | 11.2012 | 29935 | 4.91E+03 | 4.91E+03 |
| 1 | -0.5311 | -0.5360 | 1067.029 | 2.0588E-04 | 4.3019E-04 | 3.1804E-04 | 16.9677 | 36843 | 2.63E+03 | 7.54E+03 |
| 1.5 | -0.5804 | -0.5858 | 1166.246 | 2.2449E-04 | 4.7168E-04 | 3.4809E-04 | 20.2977 | 40297 | 2.01E+03 | 9.55E+03 |
| 2 | -0.6104 | -0.6161 | 1226.466 | 2.3587E-04 | 4.9664E-04 | 3.6626E-04 | 22.4600 | 42389 | 1.73E+03 | 1.13E+04 |
| 2.5 | -0.6308 | -0.6368 | 1267.576 | 2.4368E-04 | 5.1359E-04 | 3.7863E-04 | 23.9972 | 43815 | 1.56E+03 | 1.28E+04 |
| 3 | -0.6460 | -0.6521 | 1298.086 | 2.4949E-04 | 5.2611E-04 | 3.8780E-04 | 25.1700 | 44873 | 1.46E+03 | 1.43E+04 |
| 3.5 | -0.6580 | -0.6642 | 1322.217 | 2.5409E-04 | 5.3599E-04 | 3.9504E-04 | 26.1167 | 45709 | 1.38E+03 | 1.57E+04 |
| 4 | -0.6680 | -0.6743 | 1342.325 | 2.5794E-04 | 5.4421E-04 | 4.0107E-04 | 26.9185 | 46406 | 1.32E+03 | 1.70E+04 |
| 4.5 | -0.6768 | -0.6831 | 1359.891 | 2.6130E-04 | 5.5137E-04 | 4.0633E-04 | 27.6285 | 47014 | 1.27E+03 | 1.83E+04 |
| 5 | -0.6848 | -0.6913 | 1376.109 | 2.6441E-04 | 5.5797E-04 | 4.1119E-04 | 28.2920 | 47575 | 1.22E+03 | 1.95E+04 |
| 5.5 | -0.6931 | -0.6997 | 1392.798 | 2.6763E-04 | 5.6473E-04 | 4.1618E-04 | 28.9828 | 48152 | 1.18E+03 | 2.07E+04 |
| 6 | -0.7157 | -0.7231 | 1438.835 | 2.7014E-04 | 5.8938E-04 | 4.2976E-04 | 30.9175 | 49733 | 1.07E+03 | 2.17E+04 |
| 8 | -1.0800 | -1.0842 | 2164.22 | 6.2133E-04 | 6.9250E-04 | 6.5691E-04 | 71.0850 | 75411 | 1.23E+03 | 2.30E+04 |
| 10 | -1.3804 | -1.3858 | 2766.19 | 7.9214E-04 | 8.9003E-04 | 8.4108E-04 | 116.3298 | 96470 | 5.86E+02 | 2.35E+04 |

## SHIP STRUCTURE COMMITTEE LIAISON MEMBERS

### LIAISON MEMBERS

| | |
|---|---|
| American Society of Naval Engineers | Captain Dennis K. Kruse (USN Ret.) |
| Bath Iron Works | Mr. Steve Tarpy |
| Colorado School of Mines | Dr. Stephen Liu |
| Edison Welding Institute | Mr. Rich Green |
| International Maritime Organization | Mr. Igor Ponomarev |
| Int'l Ship and Offshore Structure Congress | Dr. Alaa Mansour |
| INTERTANKO | Mr. Dragos Rauta |
| Massachusetts Institute of Technology | |
| Memorial University of Newfoundland | Dr. M. R. Haddara |
| National Cargo Bureau | Captain Jim McNamara |
| National Transportation Safety Board - OMS | Dr. Jack Spencer |
| Office of Naval Research | Dr. Yapa Rajapaksie |
| Oil Companies International Maritime Forum | Mr. Phillip Murphy |
| Samsung Heavy Industries, Inc. | Dr. Satish Kumar |
| United States Coast Guard Academy | Commander Kurt Colella |
| United States Merchant Marine Academy | William Caliendo / Peter Web |
| United States Naval Academy | Dr. Ramswar Bhattacharyya |
| University of British Columbia | Dr. S. Calisal |
| University of California Berkeley | Dr. Robert Bea |
| Univ. of Houston - Composites Eng & Appl. | |
| University of Maryland | Dr. Bilal Ayyub |
| University of Michigan | Dr. Michael Bernitsas |
| Virginia Polytechnic and State Institute | Dr. Alan Brown |
| Webb Institute | Prof. Roger Compton |

## RECENT SHIP STRUCTURE COMMITTEE PUBLICATIONS

Ship Structure Committee Publications on the Web - All reports from SSC 1 to current are available to be downloaded from the Ship Structure Committee Web Site at URL: http://www.shipstructure.org
SSC 445 – SSC 393 are available on the SSC CD-ROM Library. Visit the National Technical Information Service (NTIS) Web Site for ordering hard copies of all SSC research reports at URL: http://www.ntis.gov

| SSC Report No. | Report Bibliography |
|---|---|
| SSC 468 | Development of a Structural Health Monitoring Prototype for Ship Structures Grisso, B.L 2013 |
| SSC 467 | Incorporation of Residual Stress Effects in a Plasticity and Ductile Fracture Model for Reliability Assessments of Aluminum Ship Hayden, M.J.; Gao, X,; Zhou, J.; Joyce, J.A. 2013 |
| SSC 466 | Mean Stress Assessment in Fatigue Analysis and Design Yuen, B.K.; Koko, T.S.; Polezhayeva, H.; Jiang, L 2013 |
| SSC 465 | Predictive Modeling Impact of Ice on Ship and Offshore Structures Bueno A. 2012 |
| SSC 464 | Design and Detailing for High Speed Aluminum Vessels Design Guide and Training Mish, Wh Jr., Lynch T., Hesse E., Kulis J., Wilde J., Snyder Z., Ruiz F. 2012 |
| SSC 463 | Marine Composites NDE, Inspection Techniques for Marine Composite Construction Greene, E 2012 |
| SSC 462 | Review of Current Practices of Fracture Repair Procedures for Ship Structures Wang, G, Khoo, E., ABS Corporate Technology 2012 |
| SSC 461 | Structural Challenges Faced By Arctic Ships, Kendrick A., Daley C. 2011 |
| SSC 460 | Effect of Welded Properties on Aluminum Structures, Sensharma P., Collette M., Harrington J. 2011 |
| SSC 459 | Reliability-Based Performance Assessment of Damaged Ships, Sun F., Pu Y., Chan H., Dow R.S., Shahid M., Das P.K. 2011 |
| SSC 458 | Exact Mapping of Residual Stress in Ship Hull Structures by Use of Neutron Diffraction Das S., Kenno S. 2009 |
| SSC 457 | Ship Frame Research Program – An Experimental Study of Ship Frames and Grillages Subjected to Patch Loads Daley C., Hermanski G. 2009 |
| SSC 456 | Buckling Collapse Testing of Friction Stir Welded Aluminum Paik, J.K. 2009 |